Investigation of a Novel Strategy to Promote Enhanced Visual Sensations by Electrical Retinal Implants by Means of Alternating Topological Activation of the Stimulation Electrodes

Dissertation

der Mathematisch-Naturwissenschaftlichen Fakultät

der Eberhard Karls Universität Tübingen

zur Erlangung des Grades eines

Doktors der Naturwissenschaften

(Dr. rer. nat.)

vorgelegt von

Sunetra Basavaraju

aus Bangalore, Indien

Tübingen

2020

Gedruckt mit Genehmigung der Mathematisch-Naturwissenschaftlichen Fakultät der Eberhard Karls Universität Tübingen.

Tag der mündlichen Qualifikation:	28.05.2020
Dekan:	Prof. Dr. Wolfgang Rosenstiel
1. Berichterstatter:	Prof. Dr. Eberhart Zrenner
2. Berichterstatter:	Prof. Dr. Hanspeter Mallot

Dedicated to my family.

Contents

Chapter 1

Introduction

Vision is the most valuable sense to humans, hence distortion or loss of vision leads to hindrance in performing daily life tasks which is an impairment of life. Damage to any neuronal layer (inherited or by injury) of the retina (the light sensing neuronal layer of the eye) can lead to partial or complete blindness. Worldwide researchers are investigating the potential of various approaches for vision aid including genetic and drugs, but to date no therapeutic solution is available to halt or cure blindness. Among these, electrical stimulation through microchips is employed as one of the strategies to promote visual sensations. Nevertheless, microchips implanted in human eyes, excite the retinal neurons electrically replacing essentially the light sensitive cells of the eye, have been reported to promote visual sensations in blind patients (clinical trials). Despite the pioneering success, the retinal implant requires improvements regarding temporal and spatial resolution. Hence this work address a novel strategy to improve that.

The microchip and the retina interface is complex, which requires the knowledge of the retinal anatomy and a deep understanding of the function of the neuronal circuitry to drive the electrical microchip properly. Thus, for better understanding of the most complex neuronal system. First a basic overview of the visual system

starting with the eye is briefly introduced. Initial visual image processing taking part in the retina with the help of different retinal neural layers is described. Each neural layer in the retina is specialized to decode the visual scene: For example, light sensitive photoreceptors detect the light intensities entering the eye thus, forming the primary retinal layer in visual processing. Then, different schemes of electrical retinal implants are introduced to which aim to promote visual sensations in blind patients. The concepts are at different developmental stages, there by the most advanced subretinal implant have been successful in clinical trials eliciting visual sensations in blind patients. However, all of the electrical retinal implants pose poor temporal and spatial resolution experienced by patients as "image fading", meaning long time of resting periods are required until the next image can experienced. Hence, to reduce "image fading" the implemented electrical stimulation strategy was inspired by the nature; the eye performs small eye moments, called microsaccades, to refresh the image continuously on the retina. In analogy, the electrical stimulation electrodes were activated in topologically alternating fashion leading to enhanced retinal responses. Overall the strategy is promising to promote enhanced visual sensations in retinal implant patients.

1.1 The Vertebrate Eye & the Retina

We perceive the world around us using the most fundamental of our senses, vision. The basic structural organization of the eye and the retina is similar in most of the vertebrates (Rodieck, 1998). The sclera, a flexible tissue forms the outer layer of the eyeball. It gives shape to the eyes, provides rigidity and protects the inner layers of the eye. The choroid is the vascular layer responsible for blood supply and nourishment to the retina. The transparent gel-like vitreous body covers the space between the lens and the retina. The pupil is located in front of the lens, becoming the entry point for light. Further, light reaches the retina uninterrupted, focused by the cornea and the lens as an inverted image (Rodieck,

1998). Figure 1.1 shows a schematic representation of the sagittal section of the eye and the retina. The retina is the thin neural layer at the anterior part of the eye (Figure 1.1), where the inverted image is converted into neural signals. In earlier times, it was believed that the retina only delivers filtered visual data to the higher brain regions where complex processing takes place (Webvision). But, in recent studies it has been proven that most of the processing, extraction and segregation of visual components (e.g., feature detection, motion, color, etc) from the scene takes place already in the retina and then is carried to the specific higher processing regions in the brain (Wässle, 2004; Gollisch and Meister, 2010).

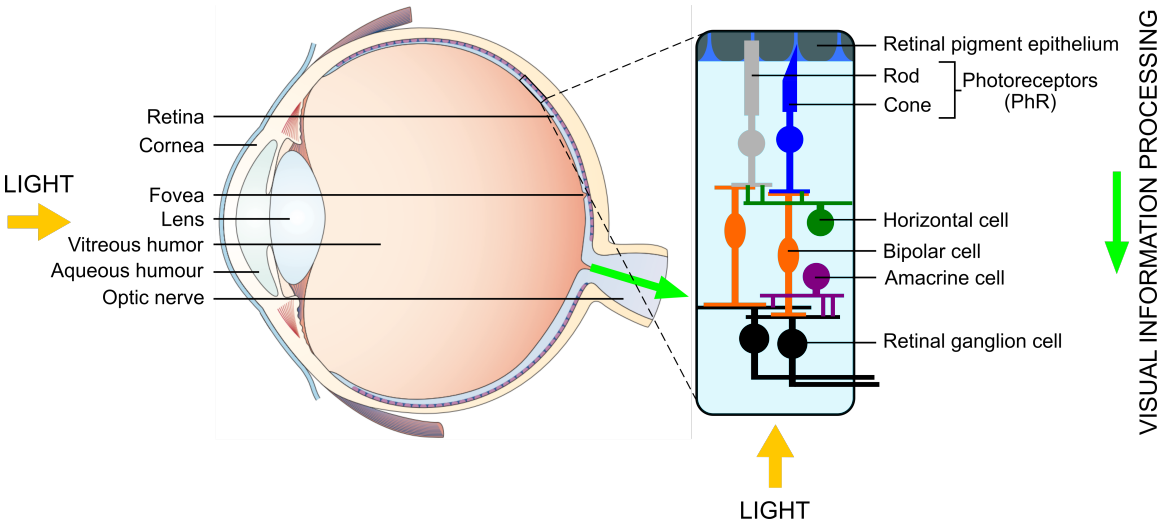

Figure 1.1: Schematic view of the eye and the retinal cross section. Eye: Adapted from Martinez-Conde et al. (2004), Retina: Adapted from Cepko (2014).

Eye movements as a mechanism to stabilize vision on the retina: A combination of eye movements such as saccades and fixation are very essential for visual perception (Land, 1999). While saccades are voluntary fast movements, fixational pauses in eye movements are involuntary, that occur between each saccade known as fixational eye movements (Martinez-Conde and Macknik, 2008; Martinez-Conde et al., 2009). Saccades reach velocities upto $900°/s$ (Fuchs, 1967; Bahill et al., 1975). Three micro movements constitute the fixational eye movements: 1) A fast flick called microsaccades (velocity = $300°/s$ and amplitude = $2°$), interleaved with 2) slow drifts, which are superimposed with 3) high frequency tremors (~90 Hz)(Figure 1.2, (Yarbus, 1967; Martinez-Conde et al., 2009)). Moreover, microsaccades are hypothized to correct the slow drifts in eye movements (Ahissar et al., 2016). Function of fixational eye movements have been studied over the years; It is said to prevent neural adaptation and fading of stationary images (Ditchburn and Ginsborg, 1952; Yarbus, 1967; Martinez-Conde et al., 2006), optimize eye position and also modulate visual processing in the brain (Martinez-Conde et al., 2004). It is said that, external visual images are moved along the path of these eye movements on the retina. Primarily, image motion due to eye movements is recognized by the retina. The effects of fixational eye movements on RGC responses have been investigated with different animal models (Greschner et al., 2002). Although saccades in mice (van Alphen et al., 2010; Krishnamoorthy et al., 2017) have been investigated, there is no clear evidence of mice having fixational eye movements. A recent study by Krishnamoorthy et al. (2017) indicated a new type of retinal ganglion cell (5-10% of the recorded population) which recognizes stimulus transitions smaller than a saccade.

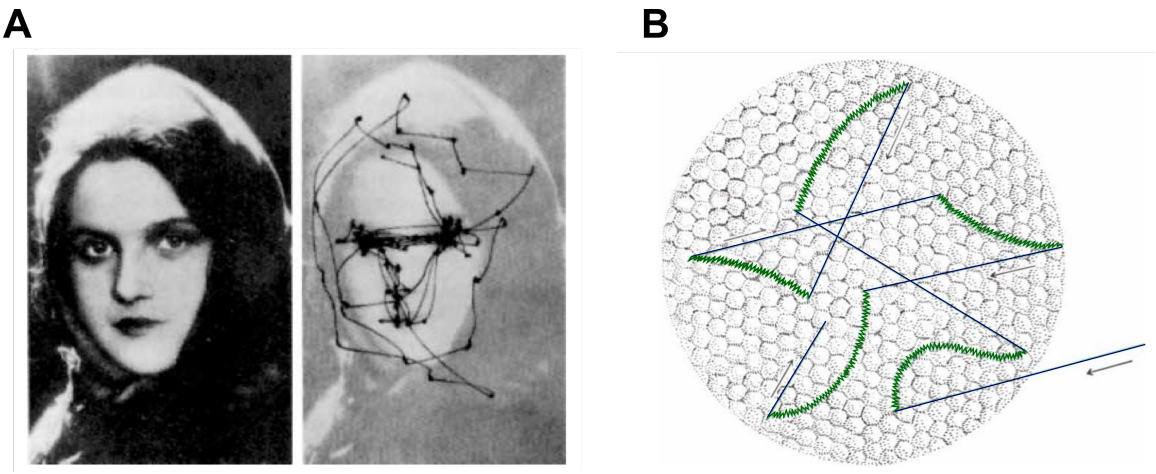

Figure 1.2: Eye movements. A) A picture of a person shown to an observer (left) and the corresponding eye movements made by the observer superimposed on the picture (right). The eyes seem to make a short move or jump and rest for a moment creating a "dot" and jump again to a new position, this cycle is continued for the examination time of one minute. The path of the jumps are the saccades and the rest positions are the fixational eye movements (Yarbus, 1967). B) Theoretical representation of fixational eye movements, explained by Pritchard (1961). Microsaccades are represented in blue, drifts with tremors are indicated in green. Each hexagonal like structure are representations of photoreceptor cells. The diameter of the retinal section shown here is ~0.05 mm, wherein the size of each photoreceptor is ~2.2 μm. The Figure is color coded only for explanation purposes, adapted from Pritchard (1961).

The Retina

The retina is composed of five major types of retinal neurons which are arranged within three neural layers and two plexiform layers. The outer neuclear layer (ONL) contains the cell bodies of the photoreceptors. The inner neuclear layer (INL) contains the cell bodies of the bipolar-, horizontal- and amacrine cells. The ganglion cell layer consists of the retinal ganglion cells (RGCs) and displaced amacrine cells. The plexiform layer divide these neural layers with synaptic contacts. The synapses in the outer plexiform layer (OPL) are formed between photoreceptors, bipolar cells and horizontal cells. The inner plexiform layer (IPL) relays information from the bipolar cells to the RGCs and also synapses are formed by amacrine cells with the RGCs. The light enters the retina through the retinal ganglion cell layer and travels through the retina before reaching the photoreceptors (in contact with the pigment epithelium at the back of the

eye). The photoreceptors transduce the light signals into electrical signals. These electrical signals are processed by the successive layers of the retina before finally reaching the RGCs. From the axons of RGCs, the output information of the retina is carried through the optic nerve to the higher visual processing parts of the brain (visual cortex) (refer to review Masland (2001); Webvision).

Photoreceptors make up the primary light sensitive functional layer of the retina categorized into two types; rods and cones (Dowling, 1987; Sterling and Demb, 2004). Rods and cones are designed to be active based on varied luminance intensity conditions in the environment (Sterling and Demb, 2004). Rods are highly sensitive to light, thus they are active in dim light conditions such as in moonless starlight (scotopic, 10^{-6} to 10^{-3} cd/m^2). As the environmental light luminance levels increase to a bright sunny day (photopic, 10 to 10^8 cd/m^2) condition, cones are activated. Both rods and cones are activated when the luminance levels are in the middle intensity ranges such as during dawn or dusk (mesopic, 10^{-3} to 10 cd/m^2, Soucy et al. (1998); Purves et al. (2001)).

Bipolar cells constitute the next level of building blocks of visual information processing in the retina (Euler et al., 2014). In vertebrate retinas, bipolar cells are broadly classified into rod bipolar cells and cone bipolar cells (Hack et al., 1999). Further, based on bipolar cell morphology and axon stratification in the IPL, one rod bipolar cell type and nine cone bipolar cell types were recognized (Ghosh et al., 2004). In studies (Shekhar et al., 2016; Tsukamoto and Omi, 2017) the classification of bipolar cells was increased to 15 types. Cone bipolar cells are further functionally classified as ON bipolar cells and OFF bipolar cells. It is at this stage that the increment and decrement in light information are identified, ON bipolar cells are depolarized at the light onset and OFF bipolar cells are depolarized at light offset (Soucy et al., 1998; Hack et al., 1999). The information from bipolar cells is carried to RGCs, the output neurons of the retina.

Retinal ganglion cells (RGCs) are the output neurons and form the final stage of information processing in the retina. Depending on their synaptic connections to the bipolar cells, earlier RGCs were broadly classified into: ON type responding to light increments, OFF type responding to light decrements and ON-OFF type responding to both light increments and decrements (Lettvin et al., 1959; Werblin and Dowling, 1969; Sterling and Demb, 2004; Farrow and Masland, 2011). In the mouse retina, morphologically they are further classified into 10-15 types (Masland, 2001; Sun et al., 2002; Rockhill et al., 2002; Kong et al., 2005; Coombs et al., 2006, 2007; Völgyi et al., 2009; Sümbül et al., 2014). Functionally classifying these broad types has been an ongoing research (Lettvin et al., 1959; Barlow et al., 1964; Carcieri et al., 2003; Devries and Baylor, 1997; Farrow and Masland, 2011; Zhang et al., 2012) eventually leading to revealing 30+ functional types (Baden et al., 2016) in recent time. Each of the functionally classified RGCs breaks down different properties of the visual scenes and projects them to different visual areas in the brain (Field and Chichilnisky, 2007). The axons of the RGCs form the optic nerve and carry the partially processed information to the visual cortex, where the distinct features of the visual scene are merged together to comprehend high dimensional visual information.

The above mentioned three retinal neuron types constitute only the vertical information pathway. Apart from these, there exists two major lateral information pathways which modulate and integrate the responses in the OPL through horizontal cells and in the IPL through amacrine cells. ***Horizontal cells*** receive inputs from several photoreceptors and modulate these inputs by providing a surround inhibition at the photoreceptor to bipolar cell synapse (Masland, 2012a). They also form synapses with each other by gap junctions, thereby increasing the spatial integration of light input (Masland, 2012a). ***Amacrine cells*** modulate responses in the IPL at the bipolar cell and RGC synapses. Amacrine cells are highly diverse in terms of their morphology and functionality, based on which there are at least 20 different classes (Masland, 2012b). It is said that, amacrine

cells are responsible for the modulation of various complex response properties of RGCs, by coupling with RGCs as inhibitory or excitatory synapses (Masland, 2012b; Euler et al., 2002).

1.2 Blindness and the Electrical Retinal Implants to Restore Visual Sensations

It has been established, that the visual system is complex and hierarchical with the retina being the primary center for visual processing. Hereditary blindness caused due to photoreceptor dystrophy, to date can neither be treated nor reversed (Hicks and Sahel, 1999; Sahni et al., 2011). Millions of people are affected by the two most common diseases characterized by the photoreceptor dystrophy; retinitis pigmentosa (RP) and age related macular degeration (AMD) (Rodieck, 1998; Kocur and Resnikoff, 2002; Hartong et al., 2006). In RP, initial peripheral vision loss occurs due to the progressive degeneration of rods followed by the degeneration of cones, leading to central vision loss (Sancho-Pelluz et al., 2008; Sahni et al., 2011). On the contrary, AMD begins with the progressive loss of central vision and then continues to peripheral regions (Coleman et al., 2008). Various research groups around the world are working towards treatment solutions for patients suffering from RP (Jacobson and Cideciyan, 2010; Zrenner, 2013; Mathieson et al., 2012) and AMD (Abd et al., 2017); including gene-therapy with optogenetics (Busskamp et al., 2012), stem-cell therapy (Singh et al., 2013), electrical transcorneal stimulation (Schatz et al., 2011) and electronic visual implants (see review Zrenner (2013)).

Amongst the mentioned approaches, electrical (E-) stimulation (stim) through E-retinal prostheses has proven to be a pioneer success in providing visual sensations to blind patients suffering from diseases caused by photoreceptor dystrophy (Zrenner, 2002, 2013). There exist three types of E-retinal prostheses based on their implantation locations in the retinal visual pathway, Figure 1.3 shows a schematic representation of the E-retinal implants.

- The ***Epiretinal implant*** is implanted in between the vitreous humour and the retina, wherein the E-stim target cells are the retinal output neural cells

(RCGs). An external camera mounted onto the glasses captures the visual scene, this information is passed onto a microchip where the visual scene is further processed. This processed visual information is transmitted to the implanted chip with E-stim electrodes which directly stimulates the RGCs (Reviews: Bloch et al. (2019); Zrenner (2013)). Different groups which are involved in developing epiretinal implants are: 1) Second Sight Medical Products CA,USA: Argus II epiretinal implants contains E-stim electrodes with a diameter of 200 μm (Humayun et al., 1996, 1999, 2012; Yanai et al., 2007; Luo and Cruz, 2016), 2) IRIS, Pixium Vision S.A.: Intelligent Retinal Implant System consists of electrodes with diameter of 250 μm (Eckmiller, 1997), 3) RWTH Aachen, Germany: EPI-RET3 retinal prosthesis with an electrode size of 100 μm. In clinical trials patients were able to perceive phosphenes, perform localization tasks and detect motion direction ((Mokwa et al., 2008), See also reviews: Bloch et al. (2019); Zrenner (2013)).

- The ***Subretinal implant*** essentially replaces the photoreceptor cells. The implantation position is between the bipolar cell layer and the pigment epithilium. This approach uses the existing retinal circuits and E-stim primarily targets the cells in the INL, the surviving bipolar cells. The implant consists of a dense array of pixels, each consisting of photodiodes and microelectrodes for E-stim. A visual scene consisting of light information enters the retina and reaches the photodiodes; imitating the photoreceptors, the photodiodes convert the light information into E-stim pulses. Through the microelectrodes, the E-stim pulses excite the successive retinal cells, further carrying out the visual information processing through the natural retinal path. Various groups developing this approach are: 1) Retina Implant AG, Reutlingen, Germany: Alpha IMS and AMS retinal implant containing 1500 and 1600 electrodes respectively, with one electrode contained in 70 μm pitch size. In results of clinical trials, patients could read letters, recognize cars, house and detect motion (Zrenner et al., 1999; Rothermel et al., 2009; Zren-

ner et al., 2010; Stingl et al., 2013, 2015, 2017), 2) PRIMA, Pixium Vision S.A.: Photovoltaic Retinal Implant consisting of one electrode in 1 mm pitch size. Clinical trail results of this implant is yet to be published (Chow and Chow (1997); Mathieson et al. (2012), See also reviews: Bloch et al. (2019); Zrenner (2013)).

- The ***Suprachoroidal implant*** is implanted between the sclera and the choroid. Though in this approach, the implant is 250 to 400 μm from the target RGCs, the implantation technique is less challenging and does not affect the retinal tissue. Unlike the subretinal implants, this implant has no photovoltaic properties, therefore a head mounted camera is used to capture the visual scene and an image processor to decode and provide E-stim patterns. Similar to the epiretinal and subretinal approaches, various groups are involved in developing suprachoroidal implants: 1) The Bionic Vision Australia containing 600 μm E-stim electrodes (Saunders et al., 2013; Ayton et al., 2014), 2) The suprachoroidal transretinal stimulation with 500 μm E-stim electrodes (Endo et al., 2018). Both of these groups are in the preliminary stages of clinical trials, where only 2 or 3 patients have been implanted (See also reviews: Bloch et al. (2019); Zrenner (2013)).

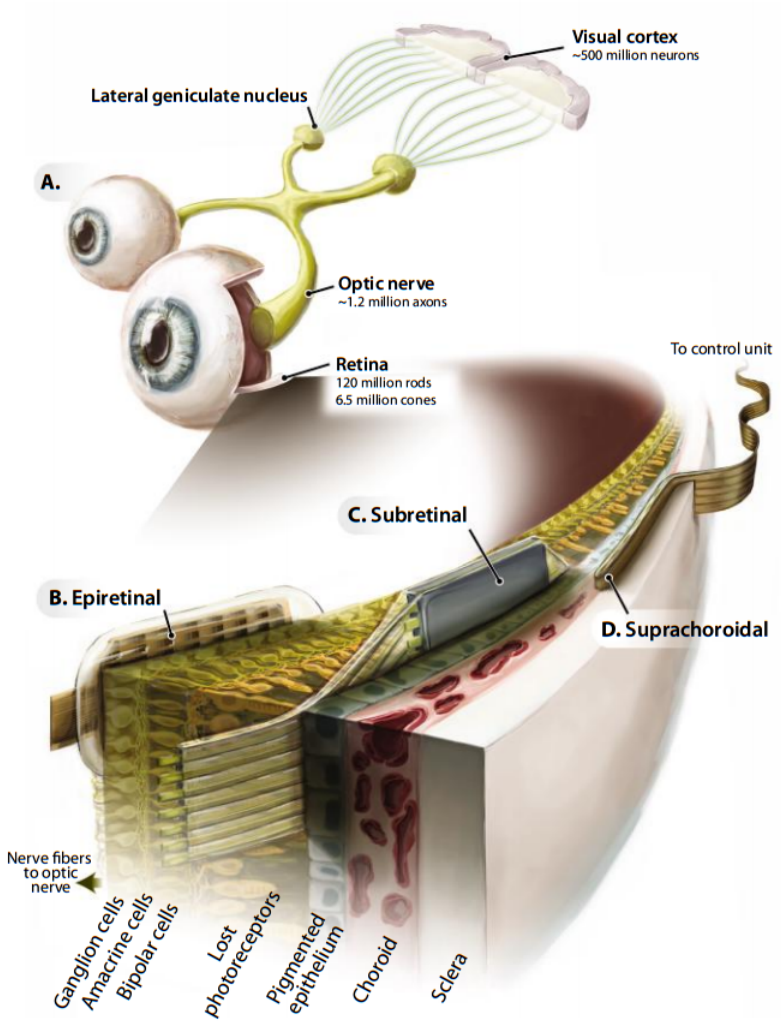

Figure 1.3: Types of electrical retinal implants. This Figure shows the three different types of electrical retinal implants based on their implantation position. From E. Zrenner, Fighting Blindness with Microelectronics. Sci. Transl. Med. 5, 210ps16 (2013). Illustration by: CREDIT: V. ALTOUNIAN/SCIENCE TRANSLATIONAL MEDICINE; (Zrenner, 2013).

1.3 Motivation

Millions of people around the world are blind due to photoreceptor dystrophies, where the progressive degeneration of light sensitive photoreceptors eventually leads to complete blindness (Kocur and Resnikoff, 2002; Hartong et al., 2006; Webvision). Electrical (E-) stimulation (stim) through E-retinal prostheses is employed as one of the strategies to promote visual sensations. Although present day E-retinal implants have shown to be pioneer works in clinical trials (describing the visual scences in terms of contrast differences and edges as seen in Figure 1.4), there exists limitations in the working potential of the implants concerning the quality of perceived visual sensations. One such limitation reported is the reduced rate of visual perception, leading to image-fading effects at E-stim frequencies higher than 2 Hz to 5 Hz (Fornos et al., 2012; Stingl et al., 2013, 2015; Hafed et al., 2016). It is also seen in the reconstruction of the described visual scene in Figure 1.4, that some visual information is lost as bright contrast gaps. In clinical studies patients have described observed phosphenes due to repeated E-stim at 5 Hz. Patients have indicated that they observed a very bright percept at the onset of E-stim, but it reduces within 0.5 s (Fornos et al., 2012). Fading of visual percepts experienced, varies from patient to patient and could also be a mechanism in visual cortex (Brindley and Lewin, 1968). Nevertheless, efforts to understand image-fading at the cellular level in the retina have been conducted in different animal models *in-vitro* (Jensen and RizzoIII, 2007; Freeman and Fried, 2011). It was stated that there is a reduction of RGC responses to repeated E-stim. The number of spikes elicited after every E-stim pulse reduced with each repetition irrespective of the E-stim frequency (Freeman and Fried, 2011).

Figure 1.4: Explained visual scene by a blind person with a subretinal implant. On the left panel is the original visual scene as observed by a healthy patient. On the right is the depiction of the visual scene as described by the blind patient with the implant. Image source: Retina Implant AG, Reutlingen, Germany.

1.4 Objectives & Approach

E-stim through E-retinal implants are used as one of the means to restore visual sensations to blind patients (Humayun et al., 2012; Zrenner, 2013). However, they are limited in their temporal and spatial resolution. As a possible reason it is reported that, due to repeated E-stim patients observe fading of visual sensations (Fornos et al., 2012; Stingl et al., 2015; Hafed et al., 2016). On the other hand, the electrode pitches in E-retinal implants are large, ranging from 70 μm to 400 μm depending on the type of E-implant (each of these E-implant pitches contain one E-stim electrode). Hence, in this work the following hypothesis is investigated: One E-stim electrode in one pitch of the E-retinal implant is experimentally replaced by multiple electrodes thereby implementing novel E-stim strategies to maintain visual sensations operating at high E-stim frequencies.

A large single-electrode representing an E-retinal implant electrode activates the cells contacting it at time point (t0). In order to activate the cells again, it is suggested that the next E-stim time point with the large electrode to be at t2. Using large electrodes to stimulate retinal cells results in lower temporal resolution, as suggested in Figure 1.5 the first E-stim time point t0 is at 0 s, the following possible E-stim time point t2 is at 2 s.

To achieve higher temporal and spatial resolution, the hypothesis of this thesis is to replace the large E-stim electrode by multiple small electrodes (Figure 1.5). Topological E-stim activation of these electrodes results in local activation of a small set of cells contacting the electrodes. Following our hypothesis wherein, the center electrode producing E-stim at time point t0 leads to activation of the small group of cells contacting it. Following which, the neighbouring two electrodes produce E-stim at time point t1 activating the neighbouring cells, thereby giving enough time for the previously stimulated cells to recover. Further, at time point t2 E-stim can be produced through the center electrode leading

to activation of the same set of cells contacting it again. This method allows to increase temporal resolution by 2 fold, first E-stim t0 is produced at 0 s, second t1 at 1 s and t2 at 2 s (Figure 1.5), also leading to higher spatial resolution by locally activating cells, as opposed to E-stim produced by one large electrode.

Aditionally, light (L-) stimulation (stim) experiments were performed to support our idea and investigate the basic parameters in more "natural" conditions. An L-stim Square-shape was presented to the retina in a stationary manner to imitate image-fading and also analogues to E-stim with large electrodes. The same L-stim Square-shape was moved on the retina to imitate micro-saccades and analogues to E-stim with small electrodes in topologically alternating manner were presented to induce non-image-fading effects. To summarize, using multiple-electrodes to stimulate the retina in a topologically alternating activation manner as opposed to conventional large single-electrodes in a stationary manner, should increase the spatial and temporal resolution of induced cell responses and in turn reduce image-fading effects.

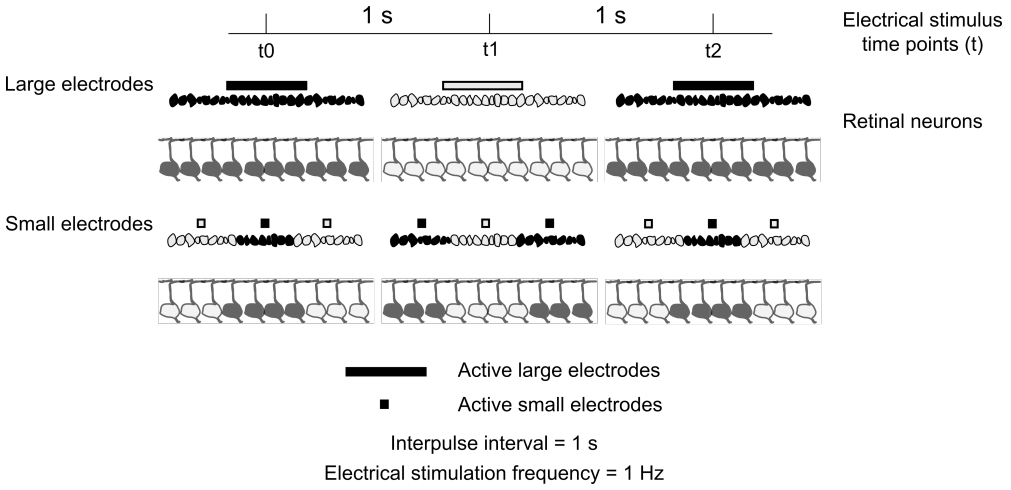

Figure 1.5: Schematic representation for the hypothesis of the thesis. Active electrical stimulation electrodes are indicated in black with the schematic of retinal neurons. Only one example of electrical stimulation frequency as 1 Hz is shown here. Figure from Haq et al. (manuscript in preparation).

Chapter 2

Materials & Methods

In this chapter, a detailed explanation of the electro-physiological experimental technique, E-stim and L-stim strategies, mouse retinal tissue preparation, RGC response recordings and respective data analyses is given.

2.1 Electro-physiological Experimental Set-up

A multielectrode array chip (MEA-chip) of hexagonal type (Multi Channel Systems MCS GmbH, Reutlingen, Germany (MCS)): Consisting of 59 circular titanium nitride (TiN) electrodes of diameter 10 μm and a center-to-center electrode spacing of 40 μm (Figure 2.1) was used in all experiments. The mean impedance of the electrodes was measured to be ~0.7 $M\Omega$. Impedance of the MEA was tested before and after each measurement using nanoZ plugged to a MEA adaptor and the MEA amplifier head stage (MCS). E-stim and L-stim strategies were presented to the explanted retina placed RGC side on the hexagonal MEA (Figure 2.1) and simultaneously the RGC responses elicited were recorded using electrodes of the MEA.

E-stim was presented using the MEA electrodes, with the signal generator STG2008 (MCS). Software used to design E-stim were MC stimulus 2 and MEA select (MCS).

L-stim was produced using a projector and was focused onto the retina using a light path consisting of different optical elements: 1) A neutral density filter (2.7 ND) to control the brightness of the L-stim, which was adjusted at 35 cd/m^2 with a background luminance of 1 cd/m^2. An automatic shutter was built using a servo motor drive and an Arduino Uno (Arduino SA, Chiasso, Switzerland) to block the light path as and when required; 2) A combination of zoom lens, mirror and an upright microscope (BX50WI, Olympus K.K., Tokyo, Japan) and a camera on the microscope were used to focus L-stim on the retina; 3) Using the advantage of MEA substrate being glass, an optical path on the opposite side was built to visualize and center L-stim on the retina with a camera. L-stim was programmed into the projector using custom made MATLAB (The MathWorks, Inc., Natick, MA, USA (TMW)) scripts, employing psychtoolbox (Brainard, 1997; Pelli, 1997) functions. Trigger signals were built into the MATLAB (TMW) code using NI USB - 6000 (National Instruments Corp., Austin, TX, USA). Figure 2.1 shows all the mechanical components of the electro-physiological set-up.

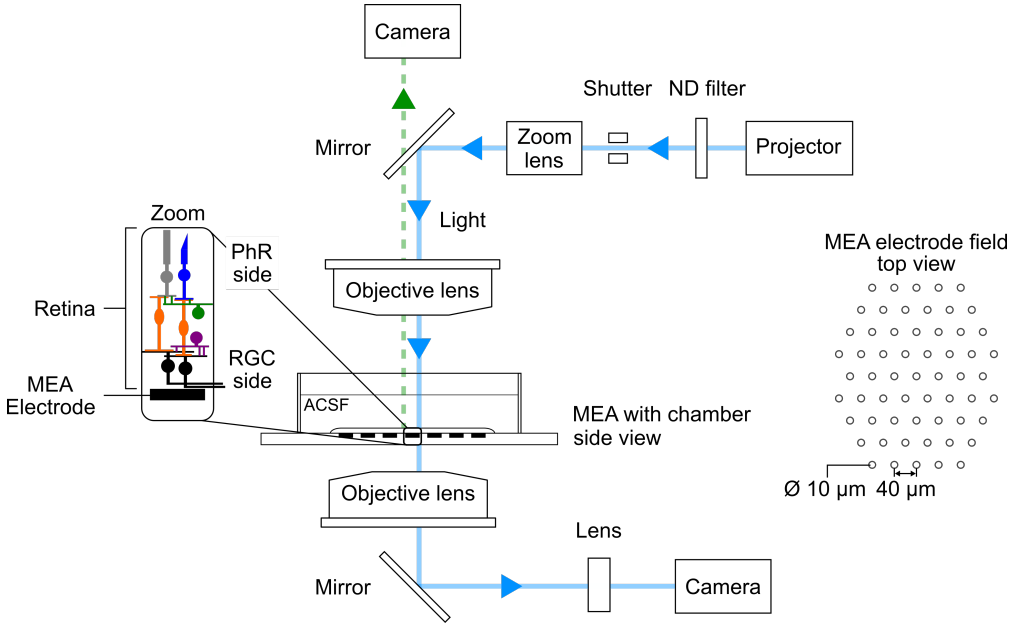

Figure 2.1: Schematic Multielectrode Recording set-up. Projector based L-stim of retinal tissue on the MEA. E-stim can be presented through the MEA electrodes. Top view of the MEA electrode field (59 electrodes in hexagonal arrangement) is shown on the right side. Abbreviations: PhR: Photoreceptor, RGC: Retinal ganglion cell, ACSF: Artificial cerebrospinal fluid, L-stim: Light stimulation, E-stim: electrical stimulation. Electrode diameter: 10 μm; Electrode spacing: 40 μm; ND: Neutral Density. Figure adapted from S. Basavaraju, A. Speck et.al, 2019 (manuscript in preparation).

2.1.1 Animals & Tissue Preparation

In this study, healthy wild type mice (C57BL/6) with ages ranging from 3 to 5 weeks were used. The animal procedures in accordance with §4 of the German law on animal protection, were supervised and approved by the Tübingen University committee on animal protection (Einrichtung für Tierschutz, Tierärztlicher Dienst und Labortierkunde). All experimental procedures were performed in accordance with ARVO statement for the use of animals in ophthalmic and vision research. Mice were carefully anaesthetized using carbon-di-oxide and then sacrificed by cervical dislocation. The eyes were quickly enucleated under dim light conditions and kept in dark condition. The eyes were then put in carbonated artificial cerebrospinal fluid (ACSF) containing (in mM): 125 NaCl, 2.5 KCl, 2 CaCl2, 1 MgCl2, 1.25 NaH2PO4, 26 NaHCO3 and 20 Glucose; pH 7.4. The dissection procedure of

the eyes to isolate retinal tissues was conducted in the ACSF medium. Eyes were hemisected, the lens and the vitreous were removed carefully without damaging the retina. Areas of the retina considered for recording were far from the cut sides or the corners touched with forceps. The dissection procedure was carried out under dim red light illumination using a dissection microscope.

2.2 Retinal Stimulation and Recordings

A dissected retinal piece was mounted on the hexagonal MEA (MCS) with the retinal ganglion cell side touching the electrodes (Figure 2.1). The electrodes of the hexagonal MEA were not only used for recording RGC responses but also for presenting E-stim to the retina. L-stim was presented using a projector incorporated in a light path used to focus the image on the retina. During the measurements, the MEA chamber was continuously perfused at the rate of 1 ml/min with carbonated ACSF using a peristaltic perfusion system (PPS2, MCS) and maintained at a temperature of ~32° C using a temperature controller (TC02, MCS).

2.2.1 Application of Light Stimulation

L-stim presented through the projector were programmed using custom made MATLAB (TMW) scripts, employing psychtoolbox (Brainard, 1997; Pelli, 1997) functions. Trigger signals were built into the MATLAB code using NI USB - 6000 (National Instruments Corp., Austin, TX, USA).

To create an user-friendly environment for L-stim programming, a graphical user interface (GUI) was custom built (Figure 2.2). L-stim shape, size, intensity and its purpose (stationary, flash or moving with different speeds in different paths) can be easily adjusted with the GUI.

Five repetitions of L-stim full field flashes of 2 s ON (35 cd/m^2) and 2 s OFF (1 cd/m^2) were presented to the retina to inspect electrode-tissue contact. L-stim induced RGC responses were collected from all 59 locations corresponding to MEA electrodes. The retinal tissue placed on the MEA was considered for further stimulation (L-stim or E-stim) only when more than 90 % of the electrode locations showed L-stim induced ON-OFF RGC responses. RCG responses correlated to light increase (ON, 35 cd/m^2) and light decrease (OFF, 1 cd/m^2) were observed. Correlated RGC responses were observed for every ON and OFF L-stim after which, the mounted retina was left on the MEA to adapt to the environment for at least 60 minutes before L-stim and E-stim measurements.

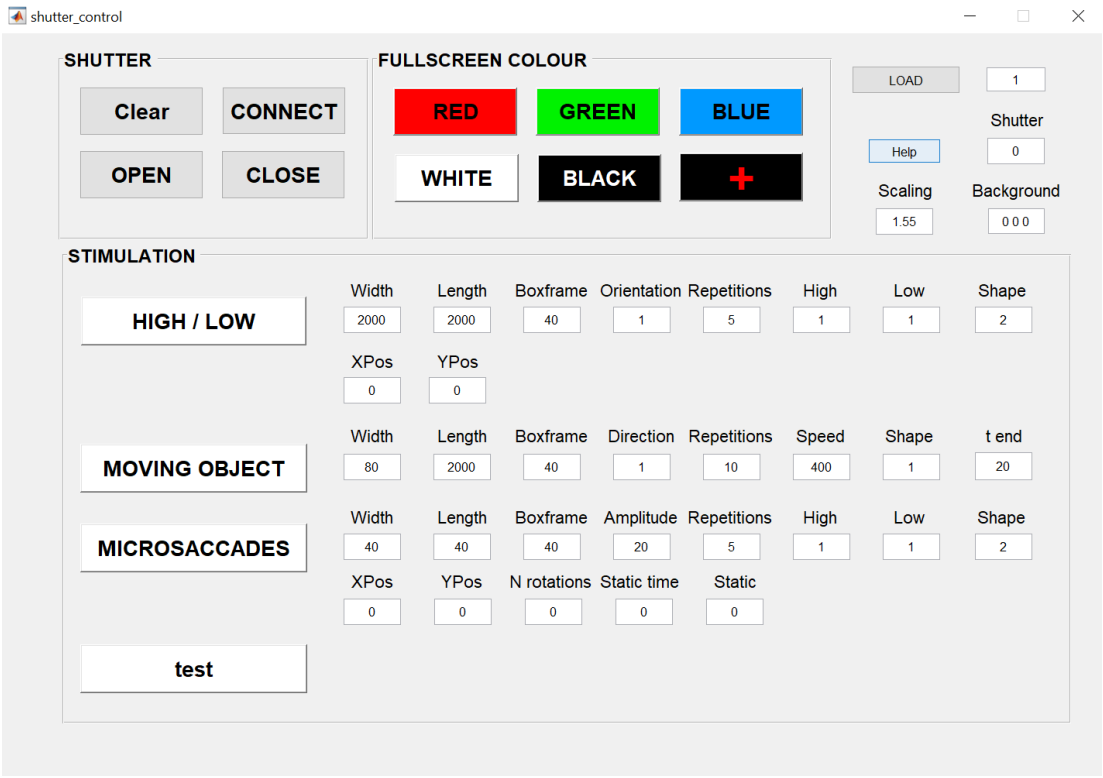

Figure 2.2: Light stimulation - Graphical user interface. It runs on MATLAB (TMW) based algorithms, interfaced with psychtoolbox (Brainard, 1997; Pelli, 1997). Text entry boxes are left to user decision, buttons are marked suggesting their respective functions. Pressing the help button opens a pop up window which provides information to the user on methods to use the graphical user interface. This Graphical user interface was developed in collaboration with Achim Speck.

Light stimulation: Square-shape Moving Along a Human Microsaccade-like Path

L-stim was presented as a Square-shape of sizes 76 x 76 μm and 152 x 152 μm. The sizes of L-stim Square-shapes were based on studies to asses the oculomotor behavior of blind people in clinical trials (Hafed et al., 2016), wherein a sqaure shape of size 2.44° was used. Therefore, the basis of the smallest L-stim Suare-shape size of 76 x 76 μm was based on Hafed et al. (2016). The larger Square-shape (152 x 152 μm - double the size of the smaller object) was used for experimental exploration curiosity. The object sizes were converted based on the following values: Human 1° visual angle represents ~300 μm on the retina (Drasdo and Fowler, 1974). This was scaled down to mouse numbers, wherein mouse 1° visual angle represents ~31 μm on the retina (Remtulla and Hallett, 1985).

The stationary Square-shape was presented for 60 s to the retina to represent fading effects. Fixational eye movement path (human microsaccade-like) was simulated based on theoretical understanding from Pritchard (1961). Various studies have shown that, humans make microsaccades with a maximum amplitude of 1° visual angle (Martinez-Conde et al., 2009). Therefore, the hMS-like paths in this thesis were programmed to cover two circular areas on the mouse retina of diameters 31 μm and 62 μm (scaled down to mouse retina based on the conversion values mentioned). Though 62 μm did not fall into the 1° visual angle of the mouse, it was used for experimental exploration curiosity. Moreover, in circular areas with diameters 31 μm and 62 μm of the hMS-like path, the longest MS length were 10 μm and 20 μm which were both less than 1° of mouse visual angle (Figure 2.3A).

The path described by (Pritchard, 1961) was turned anticlockwise in 22.5° angles 16 times, in order to have an extended time for stimulation. This new path was adjusted in diameter sizes d = 31 μm and d = 62 μm. Figure 2.3A shows the flow chart of the hMS-like path created, and the diameter sizes in

comparison to the MEA. The two Square-shapes were moved along these paths. This movement resulted in different areas covered by the Square-shapes on the MEA. Figure 2.3B shows the schematic of each Square-shape and the areas covered by the Square-shapes when moved along the two diameters of hMS-like paths. These are shown superimposed on the MEA to help visualize the relative L-stim parameters. Square-shape sizes and hMS-like path diameter values were converted and adjusted to mouse vision using numbers provided by (Remtulla and Hallett (1985)). The approximate length of one microsaccade in the hMS-like path was measured: For d = 31 μm it is 10 μm and for d = 62 μm it is 20 μm.

Mouse full saccades were measured to be of amplitudes ~13-22° of mouse visual angle with peak velocities exceeding $100°/s$ (Sakatani and Isa, 2007). One limitation with L-stim experiments was the 60 Hz frame rate of the projector, which implies the micro-movements reached a velocity of only ~$20°/s$ or ~$40°/s$, which were lower in values compared to the actual hMS velocities (Martinez-Conde et al., 2009) or even mouse saccade velocities (Sakatani and Isa, 2007). Also, the mouse flicker-fusion is 30 Hz (Schaeffel, 2017), half of the projector frame-rate.

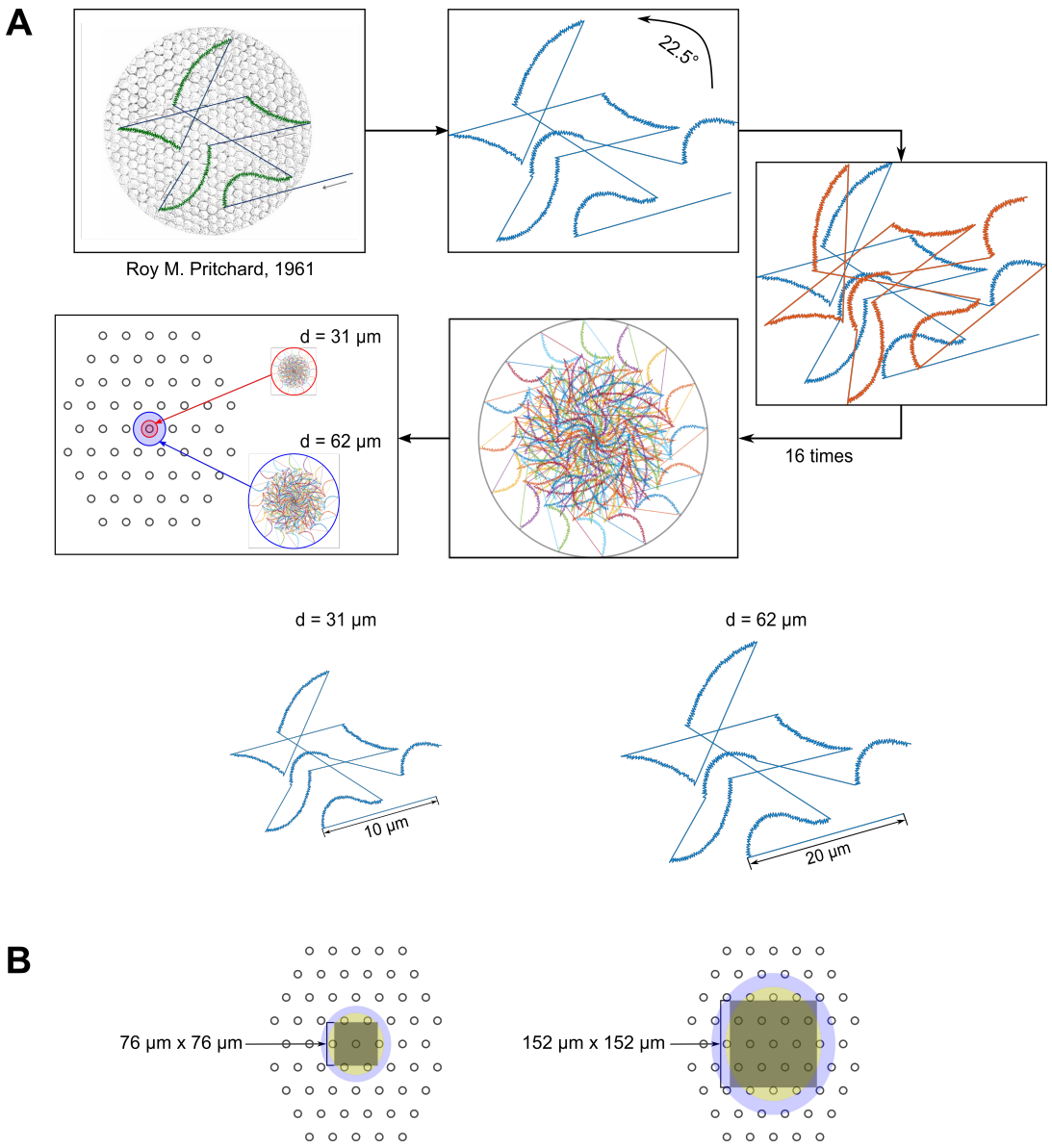

Figure 2.3: Light stimulation strategy. (A) Flow chart showing the creation of a hMS-like path, which was adapted from (Pritchard, 1961). One hMS-like path was then rotated anticlockwise at 22.5° 16 times. This whole sequence was scaled to cover a circular area having a diameter (d) of 31 μm and 62 μm (~1° and ~2° in a mouse retina Remtulla and Hallett (1985)). The light Square-shape were then moved along this pathway. In the inset approximate length of the hMS-like pattern in each diameter is shown. (B) L-stim Square-shape and the area covered by it on the MEA while moving along the hMS-like path. Square-shape of sizes 76 x 76 μm and 152 x 152 μm. Light intensity = 35 cd/m^2. Presented as stationary and moving along the hMS-like path. The yellow shaded region corresponds to the area covered by the Square-shape when moved along the path inside the 31 μm hMS-like diameter. The blue shaded region corresponds to the area covered by the Square-shape when moved along the path inside the 62 μm hMS-like diameter. Abbreviations: hMS: Human microsaccade. Electrode diameter: 10 μm; Electrode spacing: 40 μm.

2.2.2 Application of Electrical Stimulation

E-stim was presented using the MEA electrodes, with the signal generator STG2008 (MCS). Software used to design E-stim strategies were MC_Stimulus II and MEA_Select (MCS). E-stim strengths and duration presented to the retina were below the safe charge injection limits specified by the manufacturer.

Electrical stimulation Presentation using a Single-MEA Electrode

In order to understand the operational limits of the MEA system during E-stim and to procure an E-stim strength suitable for our main experiments, preliminary experiments were conducted. Retinal tissue was stimulated using a single-MEA electrode presenting monomodal cathodic E-stim strengths; -100, -300, -500, -700, -1000, -1200, -1500, -1700, -2000, -2200, -2500, -2700, -3000 mV and the pulse duration was set to 0.5 ms. The minus (-) before every E-stim strength is an indication to a cathodic pulse (Boinagrov et al., 2014). Each E-stim single-MEA electrode strategy consisted (Figure 2.4): Selected E-stim pulse strength repeated 10 times with an interpulse interval of 10 s. Each stimulus strength delivered an output current which was calculated using Ohm's Law, and respective amount of charge dissipated into the tissue was calculated as an integral of current over time (Figure 2.4 table):

$$I = \frac{V}{Z} \tag{2.1}$$

$$Q = \int I \, \mathrm{d}t \tag{2.2}$$

where I: Is the current in amperes (A), V: Applied voltage in volts (V), Z: Impedance of the electrode in ohms (Ω) and Q: is the charge in coulombs (C). All the E-stim pulses were programmed within the safe charge injection limits of the system. Mean electrode impedance was measured using nanoZ (MCS) to be ~0.7 $M\Omega$, at -3000 mV (highest E-stim strength) and a duration of 0.5 ms E-stim

pulse, elicits a current of ~4.3 μA (within safe charge injection limit; an E-stim pulse with a duration of 0.5 ms can be programmed to release current pulses upto ~35 μA). RGC responses elicited were recorded using the MEA electrodes neighbouring the E-stim electrode. A schematic representation of this pattern is shown in Figure 2.4, E-stim electrode is indicated as black with a square box and the recording electrodes are indicated as green. The calculated charge output values based on voltage strength and impedance of the electrode is shown in Figure 2.4 table.

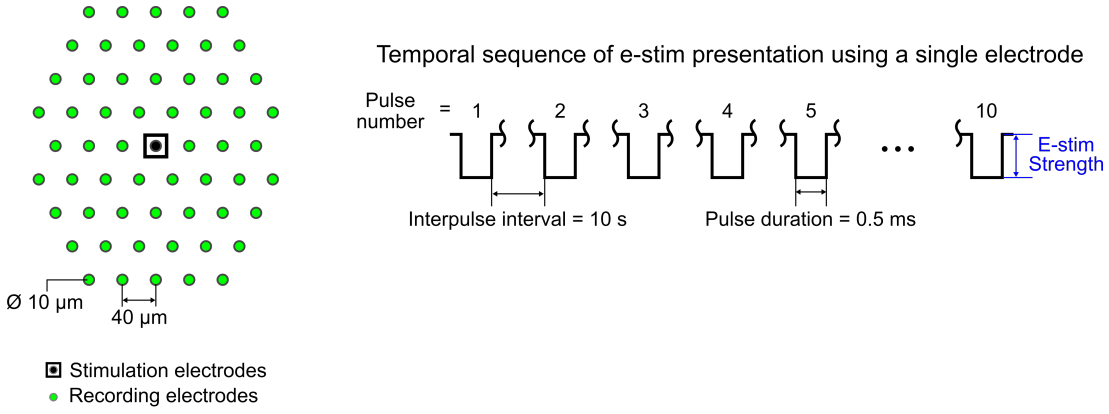

Calculated current and charge for each e-stim strength

E-stim strength cathodic (mV)	100	300	500	700	1000	1200	1500	1700	2000	2200	2500	2700	3000
Current (µA)	0.14	0.43	0.71	1	1.43	1.71	2.14	2.43	2.86	3.14	3.57	3.86	4.29
Charge (nC)	0.071	0.21	0.36	0.5	0.71	0.86	1.07	1.21	1.43	1.57	1.79	1.93	2.41

Figure 2.4: Presentation of E-stim using a single electrode. The left panel shows a schematic of the MEA. E-stim electrode is indicted as black with a black square. Recording electrode is indicated as green. The right panel shows the temporal sequence of E-stim presentation using a single electrode. The calculated value of current and charge for every E-stim strength is shown in the table below; Each E-stim strength was repeated 10 times (pulse number is numbered from 1 to 10) with a pulse duration = 0.5 ms and interpulse interval = 10 s. Electrode diameter: 10 μm; Electrode spacing: 40 μm.

Electrical stimulation Presentation using 6-e-hexagon Shape

An E-implant, e.g., the alpha AMS sub-retinal E-implant consists of 1600 E-stim electrodes (Rothermel et al., 2009). Each E-stim electrode is contained within one pitch of size 70 μm (Rothermel et al., 2009). On the MEA a single electrode of an implant is represented as a hexagon shape with a diagonal of 80 μm which is mapped using 6 E-stim MEA electrodes (6-electrode-hexagon: 6-e-hexagon). The size of the 6-e-hexagon can be compared to the size of one pitch in the alpha AMS sub-retinal E-implant. Wherein, the 6-e-hexagon representing one pitch on the MEA consists of 6 E-stim electrodes of size 10 μm as opposed to 1 E-stim electrode in 70 μm pitch of the implant. In Figure 2.5A, a schematic sketch of MEA is shown: the solid line connecting the 6-e-hexagon electrodes is the E-stim region; the dotted line surrounding the set of electrodes represents the E-stim and recording region, this section is further used in the Figure to explain E-stim strategies. E-stim was presented to the explanted retina by activating the 6-e-hexagon in three different configurations: 1) All-at-once activation of the 6 mapped E-stim MEA electrodes (6-e-hexagon), the electrodes are numbered as 1, suggesting the activation of all the E-stim electrodes at the same time, Figure 2.5B. 2) Sequential activation single E-stim electrodes placed next to each other and having the smallest distance (d = ~45 μm) within the 6-e-hexagon. Electrodes are activated as numbered, with the arrows showing the sequence of activation, 1-2-3-4-5-6 in Figure 2.5C. 3) Alternating-step activation of single E-stim electrodes spatially placed farther away from each other in "zig-zag" manner (d = ~72 μm) within the 6-e-hexagon. Electrodes are activated as numbered, with the arrows showing the steps of activation, 1-3-5-2-6-4 in Figure 2.5 D.

The E-stim frequencies presented were 1, 2, 3.3, 5, 10, 20 and 40 Hz. For All-at-once, Sequential and Alternating-step activation configurations these E-stim frequencies represented 1000, 500, 300, 200, 100, 50 and 25 ms respective

step intervals (between E-stim to E-stim). The E-stim frequencies with the 6-e-hexagon and its E-stim activation configurations were tested for 90 s. The electrodes neighbouring the E-stim electrodes in the outer circumference (in Figure 2.5, indicated in green) recorded the E-stim elicited RGC responses. E-stim was conducted at different MEA regions (1-4 as indicated in Figure 3.4) to visualize an implant-like approximation on the MEA.

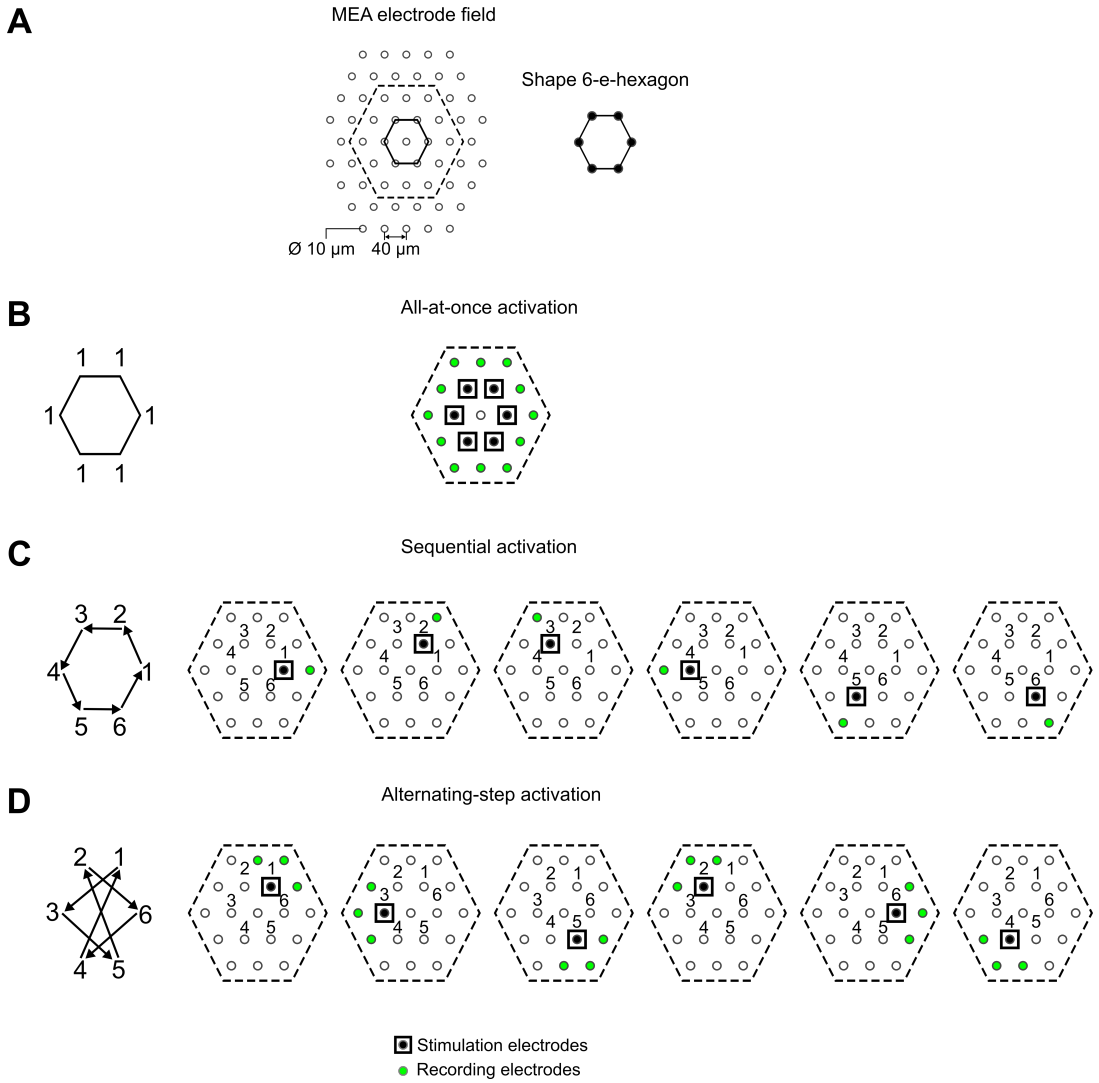

Figure 2.5: Schematic presentation of E-stim activation configurations of shape 6-e-hexagon. (A) The MEA electrode field with the electrode mapping of the shape e-hexagon with 6 electrodes (6-e-hexagon). The inner full line indicates the E-stim electrodes of the 6-e-hexagon. The electrodes between the outer dotted-line and the inner full-line are the recording electrodes. These different E-stim configurations are schematically shown. (B) Schematic representation of All-at-once activation: Simultaneous activation of all E-stim electrodes numbered as 1. (C) Schematic representation of Sequential activation: Electrodes are sequentially activated according to the numbered order (1-6). The distance between two successive E-stim electrodes is d = ~45 μm (closest to each other). (D) Schematic representation of Alternating-step activation: Electrodes are activated by skipping the immediate electrodes, thus the numbering 1-3-5-2-6-4. The distance between two successive E-stim electrodes is d = ~72 μm. To the left of each E-stim activations on the MEA, a schematic of the individual activation configurations is shown with arrows connecting the numbered electrodes. The arrows indicate the E-stim electrode activation configuration from electrode to electrode at specified E-stim frequencies (1-40 Hz). Abbreviations: E-stim: Electrical stimulation. Electrode diameter: 10 μm; Electrode spacing: 40 μm.

2.3 Data Analysis

Recorded data were high pass filtered at 200 Hz with a 2 pole butterworth filter in MC rack (MCS) and then saved in HDF5 file format. "McsMatlabDataTools" (MCS) was used to read HDF5 files in MATLAB (TMW). Further data processing was performed using custom written MATLAB (TMW) scripts. Only RGC responses which had a characteristic bimodal shape were considered for data analysis to filter out any influence from axonal stimulation (Haq et al., 2018). The error bars are standard error of the mean (± SEM).

Light stimulation

Full field flash L-stim was presented to the retina only to confirm electrode-tissue contact. L-stim hMS-like induced RGC responses were collected from the MEA electrodes and binned at 25 ms based on which the respective RCG response frequencies were calculated. Differences in the responses characteristics between stationary object L-stim and the hMS-like L-stim were characterized by averaging the RGC responses from a single and a common electrode selected at the middle of the L-stim object and the area it covered with hMS-like movement (Figure 2.3B). Examples of raw recordings are shown in Figure 3.1. A seven term gaussian curve with the function provided by MATLAB (TMW):

$$f(x) = a_1 e^{-\frac{(x-b_1)^2}{2c_1^2}} + a_2 e^{-\frac{(x-b_2)^2}{2c_2^2}} + ... + a_7 e^{-\frac{(x-b_7)^2}{2c_7^2}} \tag{2.3}$$

was fit to the RGC response histograms. The parameters of the curve fit, a: The height of the curve, b: Center position of the peak and c^2: Width of the curve with a variance σ^2 , ranging from a_1 to a_7 ; b_1 to b_7 ; c_1^2 to c_7^2 respectively for each curve (Figure 3.2) were used to describe RGC response patterns.

Electrical stimulation

Electrical stimulation Presentation Using a Single-electrode

Single electrode E-stim induced RGC responses were collected from MEA electrodes which were not used for E-stim and binned at 250 ms. For the determination of spread of E-stim induced responses dependent on E-stim strengths, MEA recording electrodes were grouped together at 40 μm bins (resulting in distance from E-stim electrode = 40, 80, 120 and 160 μm). Percentage of electrodes containing RGC responses at each distance were then plotted and a threshold was set at 25 %. A schematic representation of the analysis is shown in Figure 3.3.

Electrical stimulation Presentation Using Six Electrodes in Hexagonal Shape

In order to have a similar estimation of E-stim elicited RGC responses for all E-stim frequencies, measured RGC responses were binned at 25 ms. The performance of Sequential activation and Alternating-step activation and their comparison to All-at-once activation were evaluated using 30 trials at each E-stim frequency. For the comparison between the responses induced due to All-at-once and Alternating-step activation, average response frequencies were calculated from 10 s blocks for the recording duration of 90 s (Figure 3.9B). The difference between the response curves (black and orange) in Figure 3.7 and Figure 3.9B was determined by calculating the ratio of their respective integrals. Significance values were tested with two sample t-test *** ($p<0.001$), ** ($p<0.1$), * ($p<0.5$).

2.4 Emulation of the Electrical-retinal Implant Vision

One pitch consisting of 6 electrodes in an e-hexagon (6-e-hexagon) form on the MEA can be approximated as one pitch in an E-retinal implant (Figure 2.5 and 3.10). Therefore, a combination of pitches in an array could be emulated as an E-retinal implant. In the last section of this thesis, an approximated implant array with 56 (8 x 7) pitches were considered for simulations. Anticipation of an E-stim smiley-face depiction on the implant at relatively high E-stim frequencies was then mathematically extrapolated. The parameters of RGC response distribution (mean, standard deviation and the variance) were used as hard limit to generate computed responses based on a linear estimation (equation 2.4). A random gaussian distribution was fit to recorded RGC responses using a probability density function (equation 2.7). This was used as a feedback loop to verify if the linearly generated RGC responses fall within the 95.4 % of the gaussian distribution. This method was used for every activated pitch.

$$y = ax + b \tag{2.4}$$

$$\mu_y = a\mu_x + b \tag{2.5}$$

$$\sigma_y^2 = a^2\sigma_x^2 \tag{2.6}$$

Where a and b are constants, μ_y is the mean of the generated RGC responses, which is dependent according to the equation 2.5 and σ_y^2 is the variance of the generated RGC responses, which is dependent according to the equation 2.6.

$$f(x, \mu, \sigma) = \frac{1}{\sigma\sqrt{2\pi}} e^{-\frac{1}{2}(\frac{x-\mu}{\sigma})^2} \tag{2.7}$$

Where e is the Euler's number, μ is the mean and σ is the standard deviation.

Chapter 3

Results

3.1 Light stimulation with Micro-movements Improves the Image Refreshing Rates

The L-stim objects presented as a stationary and moving along hMS-like paths showed significant distinctions in responses. RGC responses are explained from responses seen at one electrode which is common and center to the Square-shape, moving or stationary. This was an approximation made to analyse if making micro-movements mimicking the hMS pattern on the retina helps to induce re-occurrence of responses, thus reducing fading of responses.

Diverse RGC responses were observed when the retinal tissue was presented with L-stim Square-shape of sizes 76 x 76 μm and 152 x 152 μm as: 1) Stationary object (presence of object for 60 s), 2) Moving along hMS-like path covering an area of 31 μm and 3) Moving along hMS-like path covering an area of 62 μm. Upon presentation of stationary object L-stim reveals a blast of RGC responses leading to fading of responses over time. When the same object is moved along the hMS-like pattern paths, the responses seem to reappear, suggesting the reduction of fading effects. Figure 3.1, shows an overview example of the explained response types.

The basic design of the hMS-like sequence consisted of seven micro-movements, mimicking microsaccades (Yarbus, 1967; Martinez-Conde et al., 2009), interleaved with slow curvy movements integrated with rapid movements, mimicking drifts with tremors (Yarbus, 1967; Martinez-Conde et al., 2009). When examined closer, each micro movements induced correlated increase in RGC responses; whereas the RGC responses to curvy movements with small rapid movements did not show any separate traits (Figure 3.2). These responses were fit to a seven term gaussian curve, which allowed to examine the parameters of RGC response traits. The peak RGC response position of each response did not vary irrespective of the object size and hMS sequence length. The average peak RGC response position for movement number 1-7 is as follows: 10.80±1.05, 80.81±0.79, 152.9±2.15, 199.13±1.13, 252.25±1.84, 326.28±4.4, 375.3±2.12 (Figure 3.2).

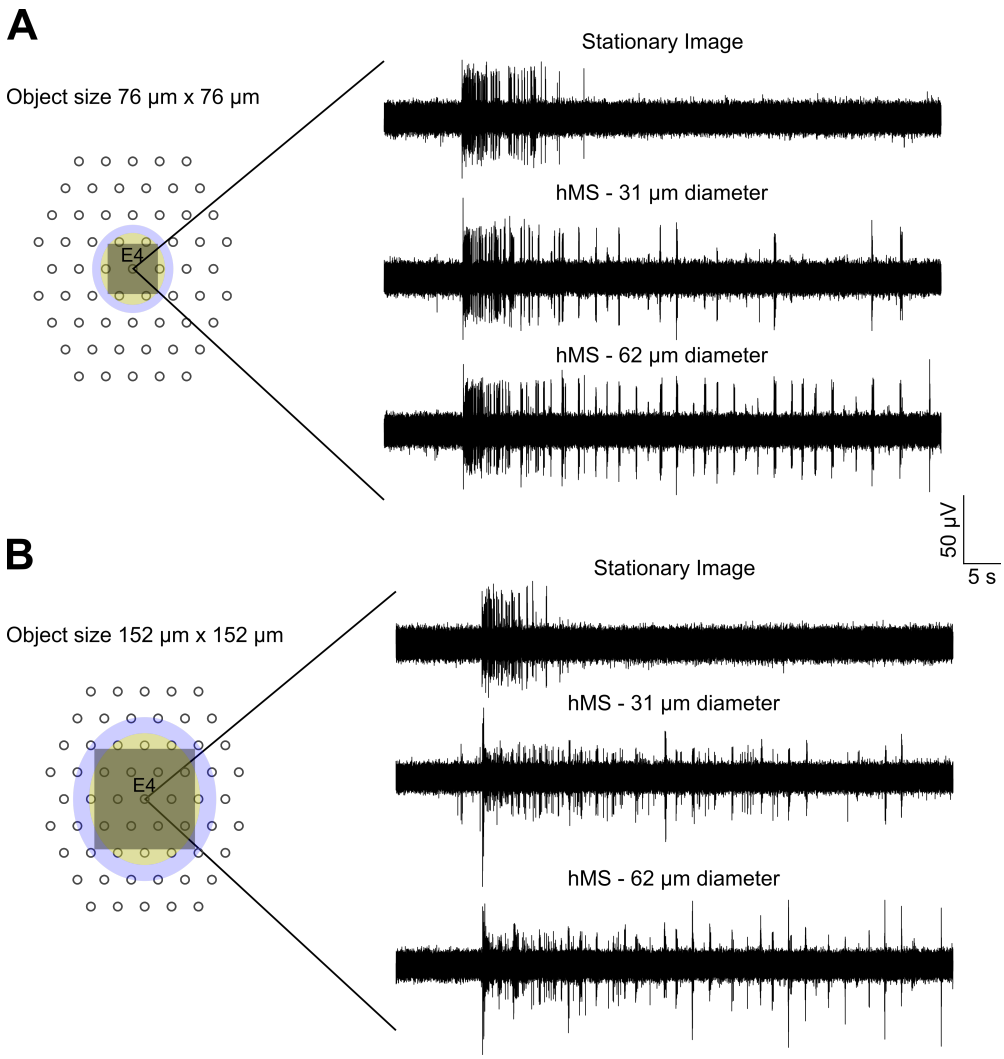

Figure 3.1: Raw RGC response examples correlated to L-stim Square-shape presented as stationary and moved along hMS-like path. (A) Left panel shows a MEA schematic superimposed with L-stim Square-shape 76 x 76 μm moving along a hMS-like path covering an area with 31 μm diameter (yellow shaded region) and covering an area with 62 μm diameter (blue shaded region). The right panel shows example raw signals recorded at electrode E4. (B) Left panel shows a MEA schematic superimposed with L-stim Square-shape 152 x 152 μm moving along hMS-like path covering an area with 31 μm diameter (yellow shaded region) and covering an area with 62 μm diameter (blue shaded region). The right panel shows example raw signal recorded at electrode E4. Abbreviations: MEA: Multielectrode array, RGC: Retinal ganglion cell, L-stim: Light stimulus. Electrode diameter: 10 μm; Electrode spacing: 40 μm.

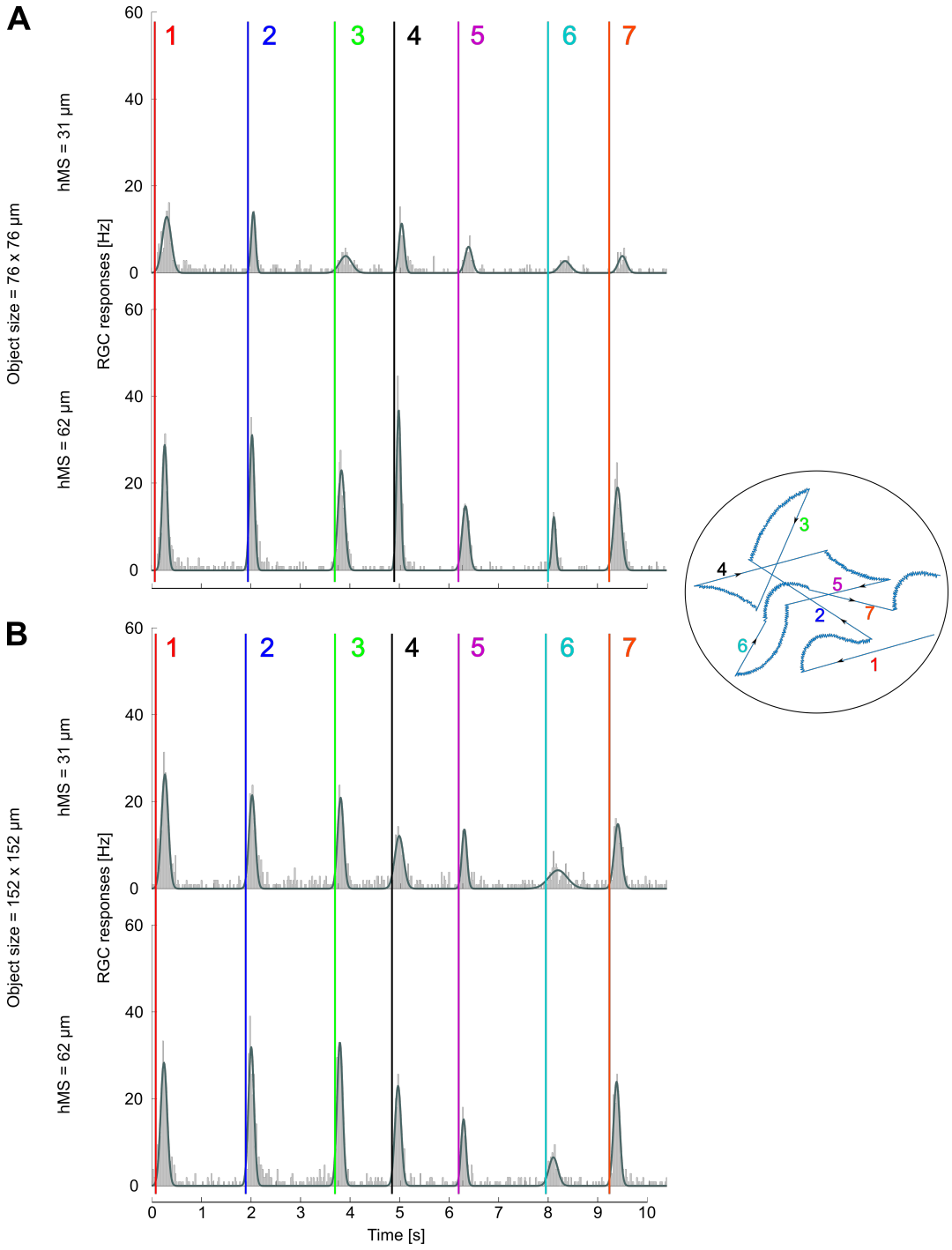

Figure 3.2: Correlated responses to L-stim Square-shape moving along hMS-like path. (A) L-stim Square-shape of size (76 x 76 μm) is moved along a hMS-like path. Average responses for each movement along both hMS-like paths (31 μm and 62 μm). (B) L-stim Square-shape of size (152 x 152 μm) is moved along hMS-like path. Average responses for each movement along both hMS-like paths (31 μm and 62 μm). In both Square-shape sizes, the corresponding movements in the hMS-like path sequence is color coded and matched to the inset (1-7, simulated hMS-like path). Abbreviations: MEA: Multielectrode array, RGC: Retinal ganglion cells, hMS: human microsaccade, L-stim: Light stimulus. Electrode diameter: 10 μm; Electrode spacing: 40 μm. The error bars are standard error of the mean (± SEM).

3.2 Electrical stimulation with Topological Alternating Activation of Electrodes Reduces Retinal Response Fading

3.2.1 Determining a Suitable Electrical stimulus using a Single MEA Electrode for Electrical stimulation

Different cathodic monomodal E-stim strengths (-100, -300, -500, -700, -1000, -1200, -1500, -1700, -2000, -2200, -2300, -2500, -2700 and -3000 mV) were presented to the retina using a single MEA electrode (E-stim design: Figure 2.4), and their respective charges were calculated. From the E-stim electrode (black with a box indicated as 0 μm in Figure 3.3), the MEA electrodes at 40 μm binning were grouped together. In Figure 3.3, green dotted lines indicate bin boundaries and the electrodes within this boundary are grouped to their respective binned groups. Percentage of electrodes within a specified bin containing single electrode E-stim induced RGC responses are plotted at E-stim strength (normalized response count). The response graphs are separated into three plots for a clear understanding of the data. A threshold of 25 % (black line in Figure 3.3) is indicated as a level of comparison. The threshold mentioned here is based on the results obtained from L-stim. In Figure 3.1 raw RGC responses elicited due to L-stim is shown, 25 % of these responses in a bin size of 250 ms is considered for the threshold of E-stim induced responses. The following results are extracted based on the three graphs (Figure 3.3).

Low E-stim strengths elicit RGC responses lower than threshold of 25 %. At E-stim strengths from -100 mV to -700 mV (with charges 0.071 nC to 0.5 nC) the normalized response counts at each bin distance are mostly below the 25 % threshold mark. Only at -700 mV (0.5 nC), normalized response counts at 40 μm bin reach the threshold with an average of 26.67$\pm$8.31 %.

E-stim strengths between -1000 mV to -1700 mV elicit local RGC responses higher than the threshold of 25 %. At E-stim strengths from -1000 mV to -1700 mV (with charges 0.71 nC to 1.21 nC) the normalized response count seem to reduce with the increase in distance from 40 μm to 120 μm and from 120 μm to 160 μm there is no significant decrease. At -1000 mV (0.71 nC) the average normalized response count at 40 μm and 80 μm bin is observed to be 45.33±9.42 % and 12.67±3.83 % respectively. Similarly, to compare this to the E-stim strength of -1200 mV (0.86 nC), the average normalized response count at 40 μm and 80 μm bin is observed to be 50±9.37 % and 17.86±5.36 % respectively. As the E-stim strength increases (-1500 mV and -1700 mV (1.07 nC and 1.21 nC)) the average normalized response count at 80 μm bin are 28.57±7.68 % and 34.62±9.33 % respectively, beyond the 25 % threshold boundary. The average normalized response count at E-stim strengths from -1000 mV (0.71 nC) to -1700 mV (1.21 nC) at 120 μm and 160 μm bin are observed to be: -1000 mV (0.71 nC): 5.33±2.28 % and 4.67±1.60 %; -1200 mV (0.86 nC): 2.14±1.10 % and 2.86±1.57 %; -1500 mV (1.07 nC): 2.14±1.10 % and 2.86±1.57 %; -1700 mV (1.21 nC): 4.62±1.76 % and 4.62±1.76 %. All these values at 120 μm and 160 μm bins are significantly lower than 25 % threshold boundary.

High E-stim strengths elicit larger spread of RGC responses higher than threshold of 25 %. Finally, at E-stim strength from -2000 mV to -3000 mV (1.43 nC to 2.41 nC) the normalized response count in most cases, not only decrease with increase in distance from E-stim electrode but also seem to cross the 25 % threshold boundary at farthest 160 μm bin. It is very clearly seen, that at E-stim strengths of -2000 mV and -2200 mV (1.43 nC and 1.57 nC) the average normalized response counts are significantly higher than 25 % threshold boundary at distances 40 μm and 80 μm bins (-2000 mV (1.43 nC): 75.38±10.30 % and 48.46±10.59 %; -2200 mV (1.57 nC): 75.83±9.89 % and 61.67±11.54 %). But, at the same E-stim strengths the average normalized response counts are closer to the 25 % threshold boundary when compared to the lower E-stim strengths (-2000

mV (1.43 nC): 15.38±5.40 % and 8.46±3.05 %; -2200 mV (1.57 nC): 24.17±8.86 % and 22.50±8.99 %). It is also seen that, at E-stim strengths of -2500 mV to -3000 mV (1.79 nC to 2.41) all the average normalized response counts are more than the 25 % threshold boundary irrespective of the distance.
The above observation suggests, an increase in the E-stim strength results in greater spread of responses across the MEA. Since a significant increase in the responses were not observed between -1000 mV and -1200 mV (0.71 nC and 0.86 nC) at distances 40 μm and 80 μm, a suitable E-stim strength of -1000 mV (0.71 nC) was chosen for two reasons. 1) For further experiments, local responses around the E-stim electrode were necessary and 2) Care had to be taken to not damage the MEA electrodes (More explained in the discussion).

Uniform spread of RGC responses is elicited around E-stim electrode

Establishing E-stim strengths and the E-stim electrode characterises lead to investigation of RGC response strength on the recording electrodes at 40 μm distance from the E-stim electrode (E-stim strength = -1000 mV). Region 1 had RGC response strengths at electrodes 1-6 respectively: 27.50±4.79 Hz, 34.17±5.83 Hz, 28.33±5 Hz, 40±11.55 Hz, 30±5.77 Hz, 25±5 Hz. No significant differences in characteristics were observed at regions 2 to 4. In a perfect recording scenario, the RGC responses were spread almost equally in all the surrounding electrodes irrespective of the stimulation region on the retina (Figure 3.4).

One limitation to the single electrode E-stim strategy was dependent on the available MEA system (MCS). Presentation of E-stim pulse through the electrode produces a large stimulus artefact following which the electrode blanks for a period of ~ 50 ms. During the blanking period, the E-stim electrode loses the ability to record responses. The blanking lasts for ~ 50 ms before the baseline noise returns to allow the electrode to record responses. Blanking time differs largely depending on various hardware features such as: E-stim strength from

the signal generator STG2008 (MCS), MC_Stimulus II and MEA_Select (MCS), between the MEA electrodes and also from MEA-chip to MEA-chip. Suggesting MEA electrodes' non linear characteristic as a function of hardware limitations. Thus, to avoid any conflict or unnecessary differences between recordings, responses were collected from electrodes surrounding the circumference of the E-stim electrode.

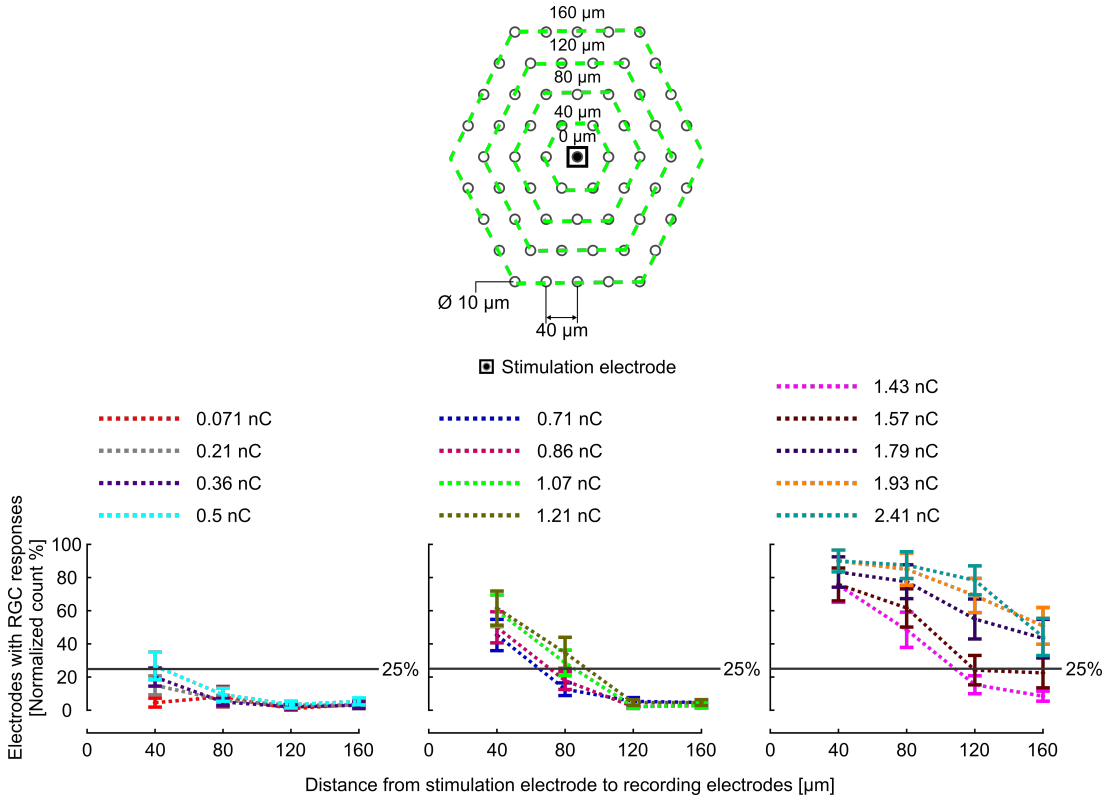

Figure 3.3: Strength & spread of RGC responses dependent on E-stim power. Top panel shows the schematic top view of the hexagonal MEA. Electrodes within a 40 μm binning distance (0, 40, 80, 120 and 160 μm) from the E-stim electrode are indicated in the area of green dashed hexagons. 0 μm electrode is the E-stim electrode mark. Three plots in the down panel show the spread of responses from the E-stim electrode at each E-stim strength (-100, -300, -500, -700, -1000, -1200, -1500, -1700, -2000, -2200, -2300, -2500, -2700 and -3000 mV). The ordinate represents the normalized average percentage of electrodes containing RGC response, the abscissa represents the distance from the E-stim electrode. Threshold of 25 % of electrodes having RGC responses is indicated by a black line. Abbreviations: MEA: Multielectrode array, RGC: Retinal ganglion cells, E-stim: Electrical stimulation. Electrode diameter: 10 μm; Electrode spacing: 40 μm. The error bars are standard error of the mean (± SEM).

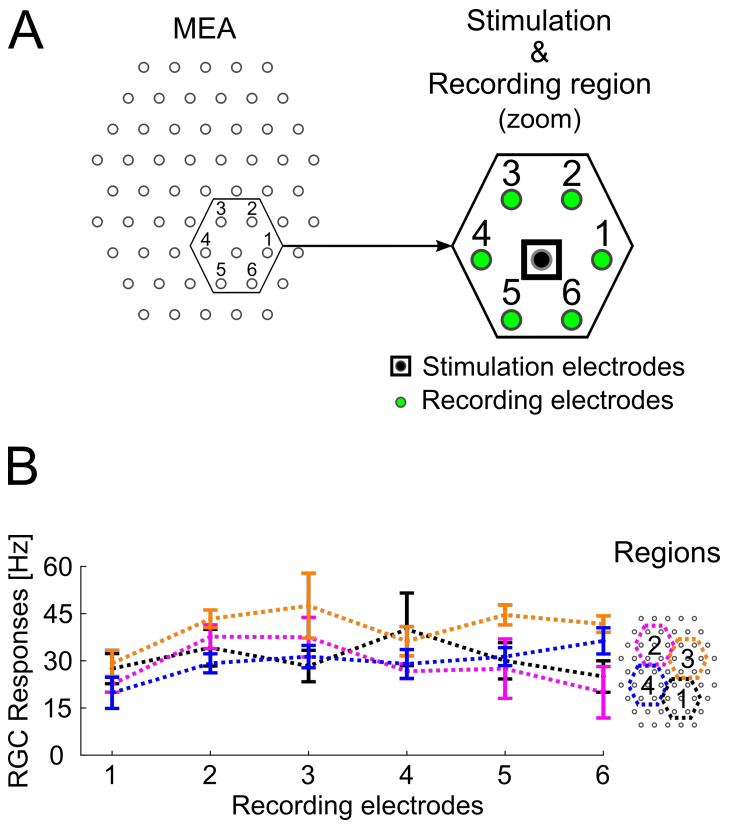

Figure 3.4: Homogeneous spread of responses with single electrode E-stim. Each color represents different recording regions on the retina, schematically shown on the MEA. Responses only at 40 μm bin are shown. The abscissa represents the recording electrode number from 1-6 and the ordinate represents the mean RGC responses in Hz. Voltage strength = -1000 mV, Pulse duration = 0.5 ms. Abbreviations: MEA: Multielectrode array, E-stim: Electrical stimulation. Error bars: ± Standard error of the mean (SEM).

3.2.2 Electrical stimulus Presentation Using 6-e-hexagon in Different Topological Activation Configurations

Results from the set of experiments conducted in the previous section a stimulus strength of -1000 mV and its elicited RGC response properties were established. This created a foundation for further experiments. An E-stim shape 6-e-hexagon (mapped using six MEA-electrodes) was presented to the retina in All-at-once, Sequential and Alternating-step activation configurations.

Due to the temporal activation configurations of the Sequential and Alternating-step, it was important to understand the respective RGC responses elicited due to each E-stim electrode (1-6) activation within the configurations. RGC responses elicited due to the activation of E-stim electrodes from 1 to 6 for the first time in Sequential and Alternating-step manner were examined in different regions of the retinal tissue. No particular E-stim dependent pattern in responses was observed within the E-stim activation configuration; in other words, the elicited responses at each recording region were independent from the influence of the previous E-stim. Figure 3.5 and 3.6 shows the distribution of RGC responses at all recording electrodes for different regions.

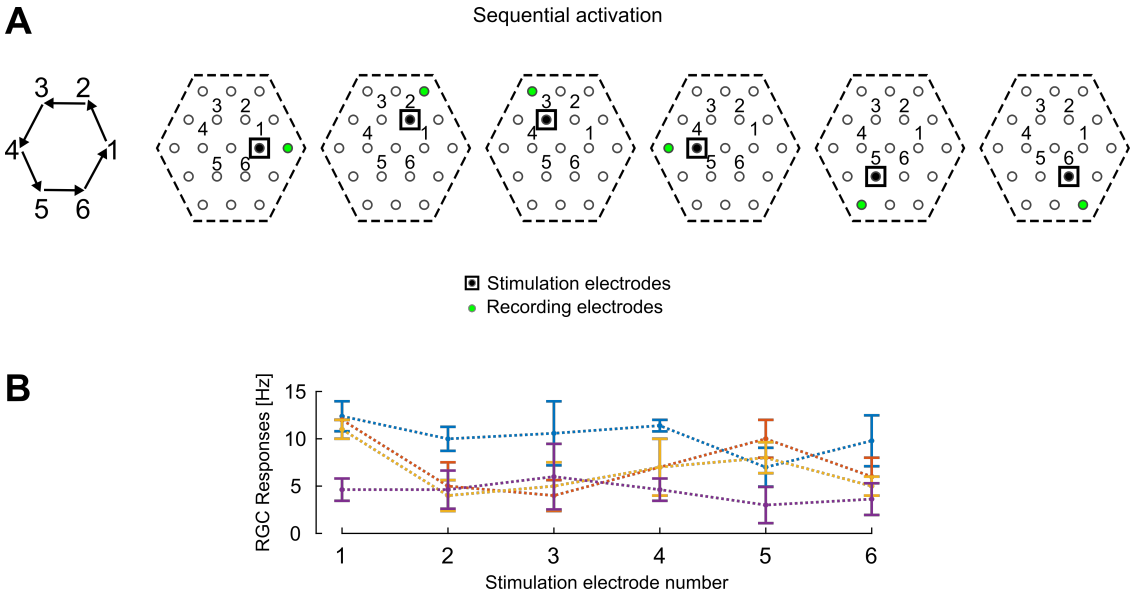

Figure 3.5: E-stim activation of the 6-e-hexagon in Sequential activation configuration and the elicited RGC responses. (A) The schematic of the six E-stim electrodes activated in Sequential configuration. (B) RGC responses elicited after the first repetition (electrode 1-2-3-4-5-6) of Sequential activation configuration irrespective of the E-stim frequency. The abscissa represents the stimulating electrode numbers 1-6 and the ordinate represents the mean RGC responses in Hz. Each coloured line in the graph represents different regions of the retinal tissue. Voltage strength = -1000 mV, Pulse duration = 0.5 ms. Abbreviations: MEA: Multielectrode array, E-stim: Electrical stimulation. Error bars: ± Standard error of the mean (SEM).

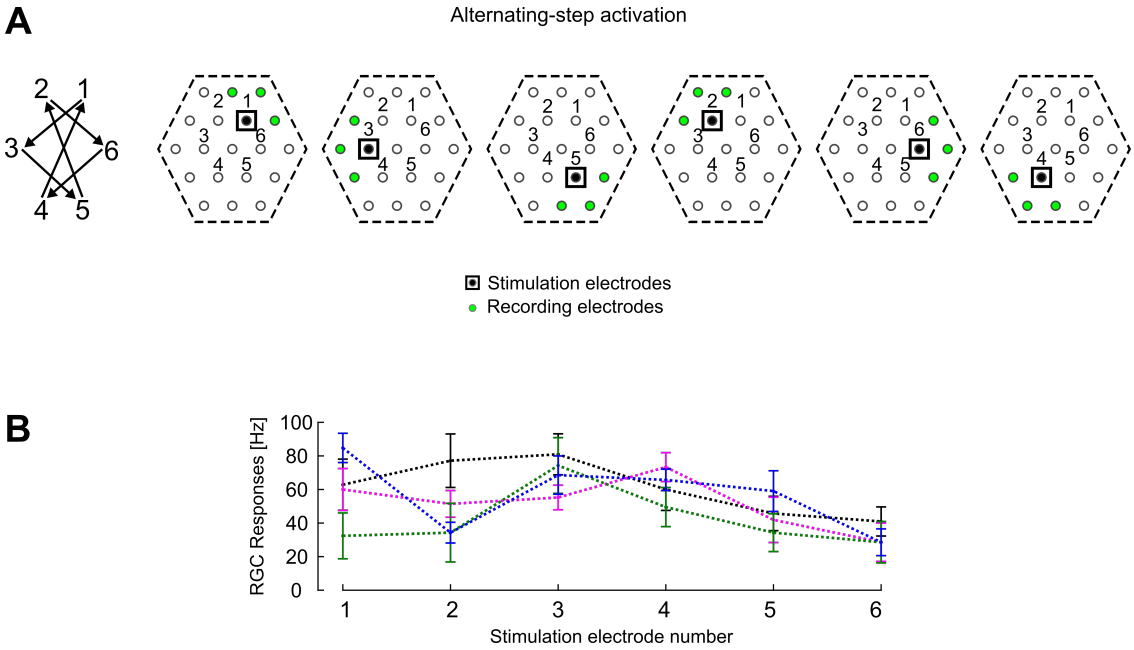

Figure 3.6: E-stim activation of the 6-e-hexagon in Alternating-step activation configuration and the elicited EGC responses. (A) The schematic of the six E-stim electrodes activated in Alternating-step configuration. (B) RGC responses elicited after the first repetition (electrode 1-3-5-2-6-4) of Alternating-step configuration irrespective of the E-stim frequency. The abscissa represents the stimulating electrode numbers 1-3-5-2-6-4 and the ordinate represents the mean RGC responses in Hz. Each coloured line in the graph represents different regions of the retinal tissue. Voltage strength = -1000 mV, Pulse duration = 0.5 ms. Abbreviations: MEA: Multielectrode array, E-stim: Electrical stimulation. Error bars: ± Standard error of the mean (SEM).

Electrical stimulation using 6-e-hexagon in Alternating-step Activation Produced Enhanced Responses as Opposed to Sequential and All-at-once Activations

The retina was stimulated by activating E-stim electrodes in the 6-e-hexagon using All-at-once, Sequential and Alternating-step configurations. Each of these activation configurations were repeated 30 times at E-stim frequencies of 1, 2, 10 and 20 Hz. In general, for the All-at-once activation configurations, RGC responses decreased with increasing E-stim frequency. Although this decrease in RGC responses was also a result of Sequential and Alternating-step activation configurations, the overall mean responses differed between activation configurations.

A considerable 87.78 % and 561.09 % improvement in responses was seen with Alternating-step as opposed to Sequential and All-at-once activation respectively (Figure 3.7). Similarly, a 264.26 % improvement in responses was seen with Sequential activation as opposed to All-at-once activation (Figure 3.7).

Responses induced through Alternating-step activation (orange curve in Figure 3.7) at a E-stim frequency of 1 Hz were 41.07±4.36 Hz, which was a 1.8-fold increase from the responses induced through Sequential activation (22.78±3.5 Hz, grey curve in Figure 3.7). Similarly, at E-stim frequencies of 2 Hz and 20 Hz 1.62-fold and 2.21-fold increases were observed respectively (Alternating-step configuration at E-stim frequencies of 2 Hz and 20 Hz elicited responses of 24.96±1.8 Hz and 6.72±0.67 Hz, Sequential at E-stim frequencies of 2 Hz and 20 Hz resulted in responses of 15.39±2.28 Hz and 3.04±0.45 Hz).

Average RGC responses induced through Sequential activation showed a 2.57-fold (Sequential = 22.78±3.50 Hz || All-at-once = 8.87±1.71 Hz), 5.81-fold (Sequential = 15.39±2.28 Hz || All-at-once = 2.65±1.04 Hz), 6.83-fold (Sequen-

tial = 4.76±0.80 Hz || All-at-once = 0.70±0.19 Hz) and 7.60-fold (Sequential = 3.04±0.50 Hz || All-at-once = 0.40±0.12 Hz) increase when compared to All-at-once activation at E-stim frequencies of 1 Hz, 2 Hz, 10 Hz and 20 Hz respectively.

Lowest average RGC responses were induced through All-at-once activation (orange curve in Figure 3.7). Which showed a 4.63-fold (All-at-once = 8.87±1.71 Hz || Alternating-step = 41.07±4.36 Hz), 9.42-fold (All-at-once = 2.65±1.04 Hz || Alternating-step = 24.96±1.80 Hz), 15.33-fold (All-at-once = 0.70±0.19 Hz || Alternating-step = 10.68±0.43 Hz) and 16.83-fold (All-at-once = 0.40±0.12 Hz || Alternating-step = 6.72±0.67 Hz) decrease in RGC responses when compared to Alternating-step activation at E-stim frequencies of 1 Hz, 2 Hz, 10 Hz and 20 Hz respectively.

In conclusion, E-stim of the retina using Alternating-step activation elicits a clear enhancement in RGC responses when compared to both All-at-once and Sequential activation. Therefore, the concept of stimulation using subsequent E-stim electrodes which are at farther distance within the 6-e-hexagon (as in Alternating-step activation) was considered as a plausible solution for future E-retinal implants.

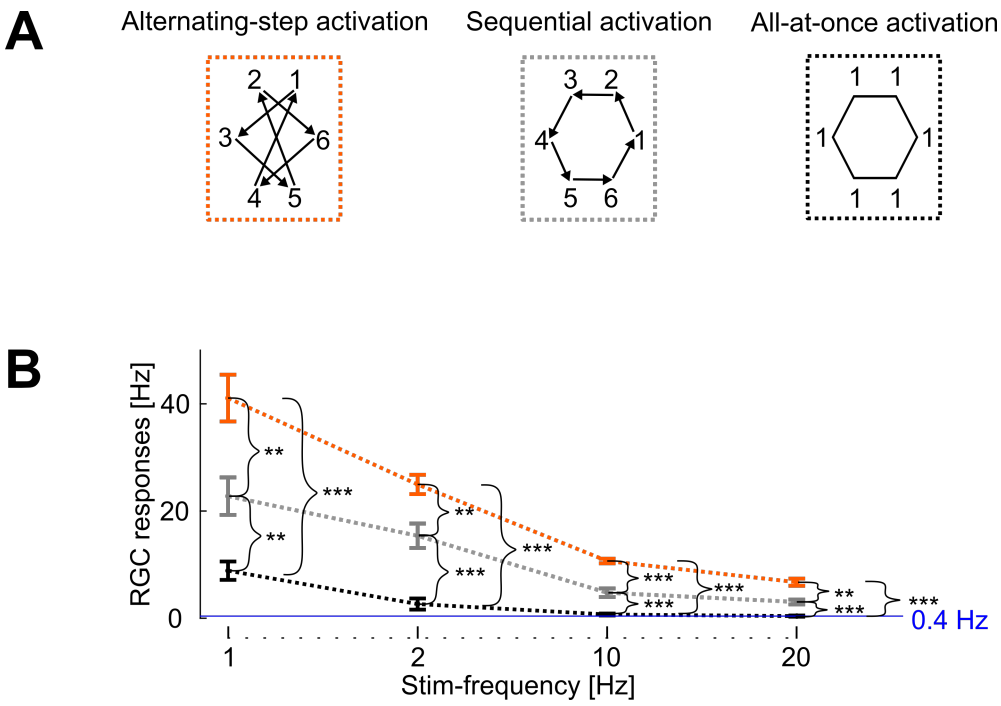

Figure 3.7: E-stim elicited RGC responses with 6-e-hexagon shape employing three different activation configurations. (A) Schematic of the three different E-stim activation configurations. The numbers indicate the E-stim electrode numbers and the arrows indicate their sequence of activation. The All-at-once activation configuration is indicated as 1 because E-stim electrodes of 6-e-hexagon are activated at the same time. (B) Average responses over 30 repetitions of All-at-once (black curve), Sequential (grey curve) and Alternating-step (orange curve) E-stim electrode activation at various frequencies (1, 2, 10 and 20 Hz) are shown. The abscissa represents the E-stim frequencies and the ordinate represents the RGC responses in Hz. The blue line shows the minimum mean response obtained (0.4 Hz). Voltage strength = -1000 mV, Pulse duration = 0.5 ms. Abbreviations: MEA: Multielectrode array, E-stim: Electrical stimulation. Error bars: ± Standard error of the mean (SEM). Significance was calculated using two sample t-test *** $p < 0.001$, ** $p < 0.1$, * $p < 0.5$.

Electrical stimulation using 6-e-hexagon in Alternating-step Activation Maintains RGC Responses for 90 s

From the previous section it was confirmed that, presenting E-stim with Alternating-step activation produced the most enhanced RGC responses. The next step was to analyse the endurance of Alternating-step activation to reduce image-fading effects, i.e., if the represented object in the pitch (6-e-hexagon) can elicit reliable responses for a relatively long period of time at a high E-stim frequency. Therefore, the E-stim was presented by activating 6-e-hexagon with All-at-once and in Alternating-step activation manner for 90 s at E-stim frequencies 1, 2, 3.3, 5, 10 and 20 Hz. For an easier understanding of the data, two plots were created: 1) A snapshot of the E-stim duration upto 1.1 s, E-stim frequency of 10 Hz, E-stim strengths of -1000 mV and -2000 mV, 2) An average at every 10 s of E-stim for 90 s, at all E-stim frequencies, E-stim strength of -1000 mV.

RGC responses induced by E-stim with All-at-once and Alternating-step activation are represented on the MEA region in Figure 3.8. The Figure 3.8 represents sample time points at 100 ms bins for a duration upto 1.1 s during E-stim of the retina at 10 Hz at -1000 mV and -2000 mV. Active E-stim electrodes at each time point are indicated with a black square around it.

An initial high response around all E-stim electrodes is observed following a reduction of RGC responses due to All-at-once E-stim activation (Figure 3.8). At t = 0 s first E-stim pulse, RGC responses are seen at all recording electrodes with a mean of 17.91 Hz and 14.91 Hz at E-stim strengths -1000 mV and -2000 mV respectively. Due to subsequent E-stim pulses a decrease in RGC responses or an absence of RGC response is observed at recording electrode locations. At E-stim strength of -1000 mV, RGC responses reduce to 7.32 Hz already at 0.1 s, which is less than half from the first E-stim pulse. At 1.1 s, responses are

reduced to a mean of 0.36 Hz which is less than 1 spike per second. At E-stim strength of -2000 mV, although all recording electrodes respond, RGC responses reduce to 8 Hz at 0.1 s. At 1.1 s, responses are reduced to a mean of 1 Hz which is 1 spike per second. All-at-once activation of this accord can be an analogues comparison to E-stim with E-retinal implants inducing image-fading effects.

E-stim of the retina with Alternating-step activation reduced the image-fading effects. At both E-stim strengths -1000 mV and -2000 mV, recording electrodes surrounding E-stim electrodes respond at every E-stim time point with reduced fading-effects. At E-stim strength of -1000 mV at 0 s, RGC response produced is 25 Hz. After stimulating the retina for 1.1 s the response produced is 18.33 Hz. At E-stim strength of -2000 mV at 0 s, RGC response produced is 20 Hz. After stimulating the retina for 1.1 s the response produced is 8.33 Hz. At higher E-stim strength a continual response is observed due to previous E-stim. Although at -2000 mV E-stim strength increases the spatial resolution, due to reasons mentioned in previous section 3.2.1, E-stim of -1000 mV was considered.

To reduce the effect of image-fading effects elicited due to All-at-once E-stim activation, the retinal explant was presented with Alternating-step E-stim activation. The responses induced through Alternating-step activation were enhanced and maintained for 90 s without any substantial decrease (Figure 3.9, orange curve) compared to the responses seen in All-at-once activation (Figure 3.9, black curve). At 1 Hz E-stim frequency, the Alternating-step responses were maintained at an average level of 25.52$\pm$0.91 Hz, which is a 3.16-fold increase from the All-at-once induced responses with an average of 8.87$\pm$2.21 Hz. Likewise, at E-stim frequencies of 2, 3, 5 and 10 Hz, an increase in responses with the following ratios was observed: 7.40-fold (from 2.65$\pm$0.69 Hz to 17.85$\pm$0.55 Hz), 14.18-fold (from 0.93$\pm$0.49 Hz to 10.59$\pm$0.45 Hz), 15.89-fold (from 0.74$\pm$0.37 Hz to 9.40$\pm$0.17 Hz) and 13.81-fold (from 0.70$\pm$0.19 Hz to 8.16$\pm$0.27 Hz) respectively. At 20 Hz E-stim frequency, even though a 2.03-fold increase with an

average response improvement from 0.40±0.12 Hz to 0.77±0.14 Hz was observed, the result was not considered relevant due to the low average RGC response (less than 1 spike per second).

In Figure 3.9, the black curve shows the responses due to E-stim of 6-e-hexagon with All-at-once activation. At 1 Hz E-stim frequency, the responses were reduced by 66.98 % (from 26.25±9.88 Hz to 8.67±1.03 Hz) already at 20 s and from 20 s to 90 s the responses do not vary substantially, but are maintained around a mean of 6.7±0.48 Hz. Analogously, at E-stim frequencies of 2, 3, 5, 10 and 20 Hz, the responses were reduced by 78.01 % (from 7.96±4.73 Hz to 1.75±0.24 Hz), 81.05 % (from 4.80±2.58 Hz to 0.91±0.24 Hz), 83.71 % (from 3.69±1.82 Hz to 0.60±0.14 Hz), 82.14 % (from 2.10±0.93 Hz to 0.38±0.13 Hz) and 69.94 % (from 1.32±0.44 Hz to 0.40±0.05 Hz) during 20 s of E-stim duration respectively. From E-stim duration of 20 s to 90 s at E-stim frequencies of 2, 3, 5, 10 and 20 Hz the responses were maintained at a mean of 1.98±0.22 Hz, 0.45±0.08 Hz, 0.38±0.05 Hz, 0.52±0.08 Hz and 0.29±0.03 Hz respectively.

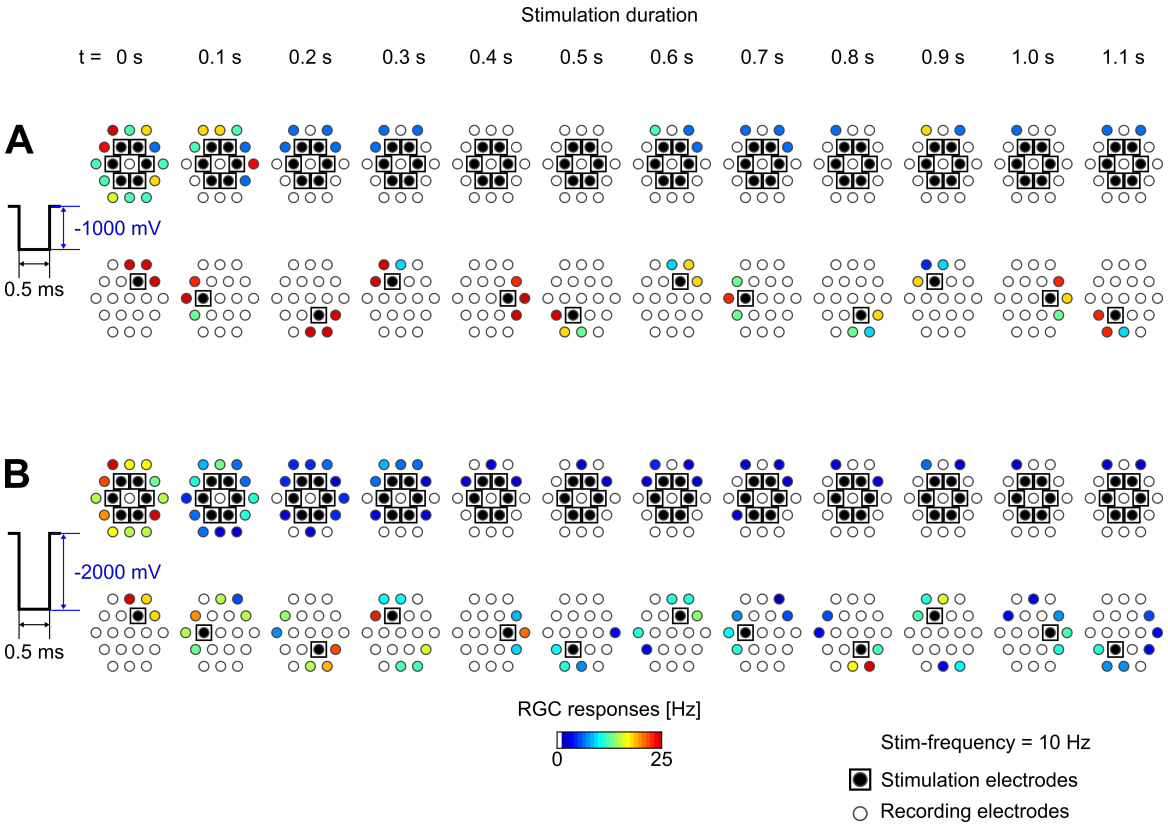

Figure 3.8: E-stim induced RGC-Performance by 6-e-hexagon with All-at-once and Alternating-step configurations. (A) RGC responses at 12 sample time points are represented as a 6-e-hexagon - stimulated by both configurations at E-stim frequency of 10 Hz and Voltage strength = -1000 mV (1.1 s E-stim duration). (B) RGC responses at sample time points are represented as a 6-e-hexagon - stimulated by both configurations at E-stim frequency of 10 Hz and Voltage strength = -2000 mV. Activated E-stim electrodes at each time point are indicated black with a black square. The color bar represents the RGC responses [Hz]. Abbreviations: RGC: Retinal ganglion cell, E-stim: Electrical stimulation. Pulse duration = 0.5 ms.

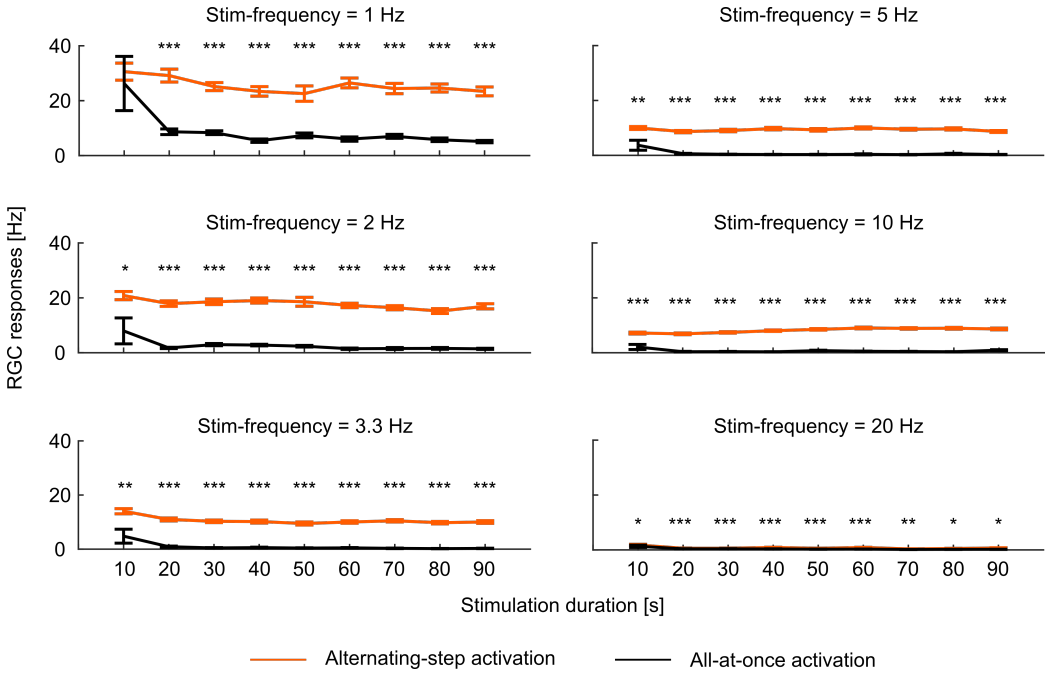

Figure 3.9: E-stim induced RGC-Performance by 6-e-hexagon with All-at-once and Alternating-step configurations for 90 s. Each panel indicates a different E-stim frequency with which the retina was stimulated using All-at-once and Alternating-step activation. Responses to Alternating-step E-stim activation for 90 s are indicated by orange curves. Responses to All-at-once E-stim activation for 90 s are indicated by black curves. The abscissa represents the stimulation duration (90 s) and the ordinate represents the mean RGC responses $[Hz]$. Abbreviations: RGC: Retinal ganglion cell, E-stim: Electrical stimulation. Voltage strength = -1000 mV, Pulse duration = 0.5 ms. Error bars: ± Standard error of the mean (SEM). Significance was calculated using two sample t-test *** p < 0.001, ** p < 0.1, * p < 0.5.

Emulation of an Electrical-retinal Implant with Novel Strategy Results in Visualisation of a Non-fading Smiley-face

Real data (RGC responses, Figure 3.8) recorded by activating E-stim electrodes All-at-once and by Alternating-step at 10 Hz was used for extrapolating and emulating the responses to visualise a smiley-face at each E-retinal implant pitch. The emulated E-retinal implant considered for this analysis was an array with 56 pitches. In Figure 3.10A the schematic representation of a smiley-face is shown on the E-retinal implant. Visualization of a smiley-face on the E-retinal implant using real data shows that the pitches containing the smiley-face information are activated. In Figure 3.10B, average responses elicited due to the 6-e-hexagon are shown as color code. When the E-stim electrodes in the pitches are activated All-at-once, the elicited responses are not only low (1 Hz) but missed information from the Smiley-face, suggesting image-fading. On the contrary, when the electrodes in the pitches required are activated in the Alternating-step method, the estimated responses depict a smiley-face with high RGC responses (10 Hz) with reduced image-fading effects. Therefore, E-stim of the retina with 6-e-hexagon in Alternating-step activation increases both spatial and temporal resolution of E-retinal implants.

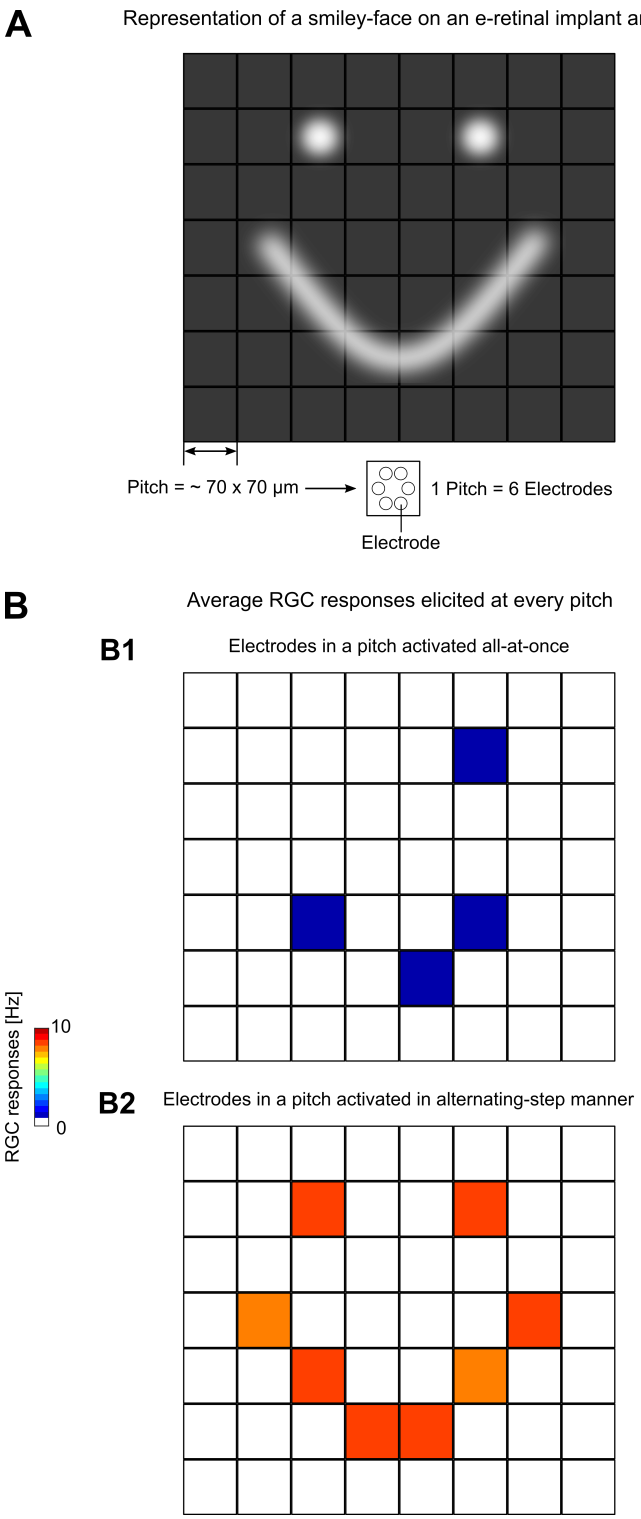

Figure 3.10: Emulation of an E-retinal implant operating using Alternating-step activation utilizing real data. (A) A smiley-face represented on an E-retinal implant array. Each square box is a pitch of ~70 x 70 μm, 1 Pitch = 6 electrodes. (B) Average RGC responses at every pitch is represented using real data from Figure 3.8 as color code in activated pitches corresponding to the smiley-face. The RGC responses are elicited due to All-at-once activation (B1) and Alternating-step activation (B2). Abbreviations: RGC: Retinal ganglion cell, E-stim: Electrical stimulation.

Chapter 4

Discussion & Conclusions

E-stim through E-retinal implantable microchips is used as one of the means to restore visual sensations to blind patients (Humayun et al., 2012; Zrenner, 2013). The electrode pitches in an E-retinal implants are large ranging from 70 μm to 400 μm depending on the type of E-retinal implant. Each of these E-retinal implant pitches contain one E-stim electrode which are used to stimulate the retina repeatedly. Due to this repeated E-stim, patients observe fading of visual sensations (Fornos et al., 2012; Stingl et al., 2015; Hafed et al., 2016), therefore resulting in poor spatial and temporal resolution. In this thesis, one E-stim electrode in 70 μm pitch of the Alpha IMS and AMS subretinal implant is experimentally replaced and mapped on the MEA by six electrodes in e-hexagon (6-e-hexagon) shape with 80 μm diagonal. Using these six electrodes in 6-e-hexagon, different E-stim activation configurations (All-at-once, Sequential and Alternating-step) were presented to the healthy mouse retina. E-stim of the retina using Alternating-step activation resulted in improved and maintained visual responses at relatively high E-stim frequencies, thereby improving the temporal resolution of the elicited RGC responses.

4.1 Image Refreshment is Achieved due to Light stimulation using Micro-movements

Primarily, in this thesis L-stim experiments were conducted to investigate the repercussions of moving a Square-shape as opposed to presenting it as a stationary shape, therefore to investigate the response from the retina in a more natural condition. This also provided an understanding of RGC responses elicited due to size of the stimulus Square-shape and micro-movements made by it. The stationary presentation of a Square-shape in L-stim is an analogous comparison to the conventional E-stim with E-retinal implants and All-at-once E-stim activation using MEA electrodes. In E-retinal implants, all the 1600 electrodes in the array simultaneously stimulate the retina (Zrenner, 2013). In All-at-once E-stim activation the electrodes of 6-e-hexagon stimulate the retina simultaneously. The static presentation of Square-shape L-stim shape resulted in RGC response bursts on the onset of stimulus before they fade away (Figure 3.1), suggesting image-fading. Such an immediate RGC response burst phenomena at the onset of L-stim was also explained in previous studies (Nirenberg and Meister, 1997; Wang et al., 2001).

To reduce this effect of image-fading, the retina was stimulated with the Square-shape making micro-movements. Presentation of L-stim with micro-movements can be an analogues comparison to the presentation of E-stim using Alternating-step and Sequential activations. Implying to stimulate the retina with high temporal and spatial resolution. Results showed correlated re-occurrences of responses for every micro-movement with length 10 μm or 20 μm, implying that it moves across ~14 or ~28 photoreceptors (size of 1 photoreceptor in mouse = ~1.4 μm (rods) and ~1.2 μm (cones) (Fu and Yau, 2007)). Although there exists evidence for mice making saccadic eye movements and compensatory head movements (Sakatani and Isa, 2007; van Alphen et al., 2010), there is no experimental evidence of mice having fixational eye movements. On a cellular

level, image motion (retinal-slip) information is conveyed by the direction selective RGCs (Baden et al., 2016). In a study with turtles (Greschner et al., 2002), it was seen that movements on the retina which have amplitudes almost equal to a photoreceptor diameter results in RGC response increase. Also, in another study with mouse, a special type of RGC was recognized (IRS cells), wherein the cells were sensitive to movements smaller than that of a full saccade or MS-like image resets (Krishnamoorthy et al., 2017).

4.2 Cathodic Electrical-stimulus Pulses Elicited Higher Retinal Cell Responses in Epiretinal Configuration than Anodic Electrical-stimulus

Research regarding E-stim with regard to E-retinal implants is an ongoing study. Wherein E-stim electrode characteristics such as; electrode materials (Onnela et al., 2011), electrode arrangement (Wilke et al., 2011; Matteucci et al., 2016), electrode size (Butterwick et al., 2007) to E-stim pulse parameters (Shyu et al., 2006; Freeman and Fried, 2011; Freeman et al., 2011; Fornos et al., 2012; Behrend et al., 2011) such as; pulse duration, pulse strength, type of E-stim pulse (cathodic, anodic, biphasic or sinusoidal) and voltage or current pulses (Chen et al., 2006; Jensen and RizzoIII, 2008; Sim et al., 2014; Twyford and Fried, 2015; Celik and Karagoz, 2018) are being studied.

In this thesis, all the elicited responses were considered without any discrimination to direct, indirect or even specific cell type responses. In different studies, it is shown that epiretinal E-stim elicits both direct and indirect responses. Direct responses (early) are elicited within ~1 ms after E-stim pulse presentation, suggesting that RGCs responding to the E-stim without the help of other retinal neural cells. Indirect responses (late) are elicited after direct responses, thus implying that the RGCs responses are network-mediated (Boinagrov et al., 2014). Such an approximation in this work is based on the goal of all E-retinal implants irrespective of the type, which is to elicit visual sensations in blind patients. The technology today achieves this goal by presenting the retina with E-stim pulses. These E-stim pulses do not target different functional cell types, on the contrary stimulate the targeted layer of cells (bipolar cells or RGCs or the suprachoroid region) without any bias.

Further, the RGC side of the retina was in contact with the MEA elec-

trodes, thus the E-stim was presented in the epiretinal configuration. The results of the preliminary experiments revealed that cathodic pulses elicited more RGC responses as opposed to anodic pulses which elicited no responses (results not shown). This result is in accordance with previously conducted studies (Boinagrov et al., 2014; Haq et al., 2018). An anodic E-stim pulse elicits higher RGC response rates at lower thresholds while stimulating bipolar cells as contrary. This type of E-stim assumes that the available retinal neurons are healthy and uses the natural pathway to elicit RGC responses as shown in Haq et al. (2018). Biphasic E-stim pulses, a dependency of responses to the parameters of cathodic and anodic phases are explained in studies (Ahn et al., 2015; Nakano et al., 2018). The advantage of such a stimulus is that, it can be used to target any part of the retinal circuitry by modulating its strength and duration. Stimulating the retina with cathodic pulses elicited higher RGC responses at lower thresholds as compared to anodic pulses (Boinagrov et al., 2014). Based on the results and the literature mentioned in this section, a cathodic pulse was chosen for epiretinal stimulation and the purpose of this study.

4.3 Spread of RGC Responses Dependent on Electrical stimulation Strength

In order to find the E-stim strength suitable for our experimental set-up, a range of cathodic E-pulse strengths were investigated. The goal of such experiments in this study, was to elicit RGC responses locally around the E-stim electrode. It was also important to achieve this result with a threshold limitation of 25 %. This threshold was determined on the results obtained from L-stim, wherein 25 % of the raw RGC responses elicited due to L-stim in a bin size of 250 ms was considered. These experiments revealed that E-stim strength of -1000 mV resulted in RGC response spread of upto 80 μm (with one E-stim electrode or more). The RGC responses at the 40 μm distances was also more than the threshold level of 25 %. The responses decreased with increase in distance, which was in agreement

with previous E-stim studies (Stett et al., 2000, 2007) and also in subretinal stimulation (Haq et al., 2018). For further experiments, it was important to have local responses and also to maintain the condition of MEA electrodes, therefore a stimulation strength of -1000 mV was optimum (see chapter 3.2.1).

As already mentioned in results, the lack of possibility of E-stim electrodes to record again became a limitation in this thesis. Working around this issue, locally surrounding electrodes in the outer circumference and with closest proximity to the E-stim electrode were considered for analysis (40 μm and ~45 μm). It was also observed that, after ~10 repetitions of the selected E-stim pulse with 10 s inter pulse interval, electrodes were able to record again. This behaviour of the E-stim electrode was disregarded in analysis of E-stim presentations to procure unbiased E-stim response characteristics.

In conclusion, E-stim pulses used in this thesis were kept within the bounds of already gained knowledge and further developed and used to reduce induced image-fading effects with better spatial and temporal resolution.

4.4 All-at-once Activation Induces Image-fading Effects

After establishing an optimal E-stim strength using a single MEA electrode, RGC responses elicited due to E-stim using 6-e-hexagon shape was investigated. The 6-e-hexagon of size 80 μm mapped on the MEA was an approximate replacement of one E-stim electrode in one pitch of the Alpha IMS and AMS subretinal implant of size 70 μm (see Figure 3.10, Rothermel et al. (2009)). The E-stim of 6-e-hexagon was presented to the retina in three different activation configurations: All-at-once, Sequential, Alternating-step.

It is to be noted that, further before each E-stim experiment L-stim was presented to the retina to cross check the retina-electrode contact in order to discriminate and exclude "bad-contact" results from E-stim induced fading.

At first All-at-once activation was used to E-stim the retina, this configuration was an imitation of the E-retinal implant stimulation. A decrease in responses occurred when the E-stim electrodes were activated All-at-once, this result was expected and in accordance to what was observed in E-stim experiments conducted by other groups (Jensen and RizzoIII, 2007; Ryu et al., 2009; Freeman and Fried, 2011; Freeman et al., 2011). In these studies, the fading effect was explained at a cellular level where the RGCs desensitized with every reoccurring and a specific number of E-stim pulses with dependence on E-stim frequency. Desensitization of RGC responses, as per conducted single electrode experiments seem to be more of local phenomena than global. These studies only noted the effects over a certain number of E-stim pulses, but our interest was to see if these responses were maintained over a course of time. Therefore, in this thesis we investigated and observed the behaviour of RGC responses over 90 s of E-stim.

Not only was the reduction of responses seen in animal tissues, but was also observed during clinical trials performed with the Argus II (Second Sight Medical Products, Inc., CA, USA) epiretinal implant (Fornos et al., 2012), where the visual sensations of the patients started to fade away within a few seconds.

4.5 The Novel Topological Electrical stimulation Strategy Reduces Image-Fading Effects

As a first pass analysis, it was important to investigate RGC responses elicited within the Sequential and Alternating-step activation configurations (first time E-stim from 1-6 electrodes, Figures 3.5 and 3.6). This was experimented by stimulating the retina at different locations. This resulted in no reduction of responses within E-stim configurations. Further, with the used electrode configuration of the hexagonal MEA (electrode d = 10 μm, electrode spacing = 40 μm), it was important to design a reasonable E-stim electrode configuration. This was also discussed in Stett et al. (2007). Subsequent E-stim electrodes which are very close to each other will cause fading effects in the retinal responses or electrical cross talk (Behrend et al., 2011; Matteucci et al., 2016). When the E-stim electrodes are too far apart, the desired object could be lacking information. Based on our observations we suggest that the distance between E-stim electrodes used for subsequent stimulation, should be as large as possible while being as small as necessary. Comparing the hexagonal E-stim electrode size and arrangement with the electrode pitch sizes of the E-retinal implants (ranging from ~70 μm to ~300 μm): 6 E-stim electrodes (10 μm each) in the 6-e-hexagon fits into approximately one electrode pitch of the E-retinal implant (~70 μm), thus increasing the spacial resolution. By alternatingly activating these electrodes, avoids overstimulation of same retinal regions, leading to less fading-effects at relatively high E-stim frequencies, thus increasing the temporal frequency.

Further, 31 μm on the mouse retina correspond to 1° of visual angle (Rem-

tulla and Hallett, 1985). A mouse visual acuity is 0.5 cycles/degree (Prusky et al., 2000). The 6-e-hexagon E-stim electrode arrangement (represented with 6 electrodes (Figure 2.5A) with a diagonal of 80 μm can be considered as a relatively local stimulus (calculated using the numbers from Remtulla and Hallett (1985); Prusky et al. (2000)). This selection of a 6-e-hexagon was also backed up by the preliminary L-stim Square-shape (76 x 76 μm) making micro-movements with hMS-like path. Re-occurrences of RGC responses were produced at same retinal locations when the Square-shape was moved along 10 μm or 20 μm paths.

To overcome the demonstrated fading effect due to All-at-once activation, a novel E-stim configuration was used. The healthy mouse retina was presented with E-stim by activating electrodes in a Sequential and Alternating-step activation for 10 repetitions. Before the presentation of 6-e-hexagon using Alternating-step activation, presentation of Sequential activation was investigated. Although Sequential activation configuration elicited higher RGC responses compared to All-at-once activation it did not perform better than Alternating-step activation. One interpretation of this result could be the distance between two consecutive E-stim electrodes is small (d = ~45 μm) defined by the high spatial resolution of the hexagonal MEA. The retinal regions in proximity to two consecutive electrodes are being repeatedly stimulated, reducing spiking recovery time and therefore resulting in local fading effects. The two electrodes not considered for analysis elicited responses to only one of the E-stim electrodes shared. For example, electrode between E-stim electrode 1 and 2, had influences from both E-stim electrodes. We accounted for this in the analysis by including responses only from those recording electrodes which had less influence from the next consecutive E-stim electrode (see methods). Therefore, for the analysis of RGC responses elicited due to E-stim by Sequential activation, only RGC responses at one electrode were considered, whereas for the analysis RGC responses elicited due to Alternating-step activation, average RGC responses from three electrodes at the outer circumference was considered (Figure 2.5 and Figure 3.5).

4.6 Alternating-step Activation Provides Enhanced Visual Responses for Electrical-retinal Implants at High Temporal Resolution

During Alternating-step activation, the RGC responses were observed to be maintained for the whole 90 s till 10 Hz (100 ms step interval) E-stim frequency. This observation underlines a drastic improvement when compared to activating the electrodes All-at-once. Also, comparing the Alternating-step activation to state-of-the-art E-stim methods (Zrenner, 2013; LanYue et al., 2016), we detected an accountable enhancement in the responses. In clinical trials of the electrical subretinal implant (Alpha IMS, Retinal Implant AG), the time for phosphene perception was ~0.5 s with 5 Hz E-stim frequency (Zrenner et al., 2010; Hafed et al., 2016). On the contrary, by activating E-stim electrodes in Alternating-step manner tested in this thesis, the responses were maintained for 90 s not only at 5 Hz but also at 10 Hz E-stim frequency.

In early clinical trials of the subretinal implant (Alpha IMS, Retinal Implant AG), a relation to E-stim frequency and electrode spacing was evaluated (Wilke et al., 2011). Here, it was suggested that with an electrode spacing of greater than 790 μm and an E-stim frequency of ~6.5 Hz, avoided fading to a large extent. In the outcome of this thesis, we observe a large improvement when the consecutive E-stim electrode distance is greater than ~72 μm and ~10 Hz or 20 Hz E-stim frequency already induced reduced fading effects.

Stimulating the retina with Alternating-step configuration, we were able to maintain RGC responses for a time course of 90 s at E-stim frequencies of 10 Hz. When compared to the 30 Hz flicker-fusion frequency of a mouse (Schaeffel, 2017), these stimulation frequencies appear high with a ratio of 33.3 %. In relation to the 55 Hz flicker-fusion frequency of a human (Schaeffel, 2017), it could be

speculated that the upper limit of the topologically alternating E-stim frequencies could be different. E-stim related flicker-fusion was measured in humans and was reported to be 50 Hz and 40 Hz (Humayun et al., 1999).

Further, the Alternating-step activation was tested with a double-bar, just as a proof of principle. The double-bar was presented to the retina using the topologically alternating E-stim Alternating-step pattern for 90 s at different E-stim frequencies (1, 5, 10, 20 and 40 Hz). The RGC responses elicited due to Alternating-step activation at various frequencies (1 - 40 Hz) showed a clear distinction of 2 bars in most cases. Importantly, the double-bar was observed at 90 s at an E-stim frequency of 20 Hz. The larger double-bar was presented by activating E-stim electrodes All-at-once as a control stimulus, the responses here were visible at t = 1 s, but they faded away completely before 10 s already at 2 Hz E-stim frequency (The data was a part of Speck et.al., 2019 data not shown.). Therefore, the method suggested in this thesis is not confined to small shapes.

4.7 Implementation of Alternating-step Activation to Electrical-retinal Implants Promotes Fading-free Electrical-vision

The retina was presented with E-stim using 6-e-hexagon in Alternating-step activation. This was an alteration from Sequential activation by increasing the distance between two consecutive E-stim electrodes within the 6-e-hexagon to ~72 μm, which compared to recent E-retinal implants (Rothermel et al., 2009; Daschner et al., 2018) is approximately the size of one electrode pitch. Thereby leading to extrapolation of recorded RGC responses to simulate a simley-face on the surface of the E-retinal implant (56 pitches). In this example, one pitch of size 70 x 70 μm contained the six mapped electrodes as a 6-e-hexagon. Each pitch functions as a unit within which, the topologically alternating E-stim strategy is used. This was also tested in the MEA used for this thesis, wherein

different regions representing pitches each with six electrodes were programmed to stimulate in topologically Alternating-step activation (see 3.4). Since the MEA consisted of only 59 electrodes used for both stimulation and recording, only four non-overlapping regions could be achieved. Based on real recorded data, a smiley-face on an example E-retinal implant was emulated. To conclude, stimulating the retina with Alternating-step E-stim activating helped to overcome the obstacle of overstimulating the same retinal regions, which leads to visualize the performance from a broader perspective.

Representing E-retinal implant pitches with multiple E-stim electrodes as opposed to presenting E-stim through a single electrode to decode RGC responses is the main approximation of this thesis. Therefore, this was tested first in a simple healthy mouse modle without encountering any cellular level complications. Such mouse models are established and ideal for experimentation (Chang, 2013). Disease mouse models increases challenges due to retinal remodelling (Jones et al., 2016), hyperactivity of RGC responses (Stasheff, 2007) and also oscillatory behaviour of spontaneous responses (Haq et al., 2018). Moreover, patients are implanted on at a later stage of degeneration, when they barely have any light perception. Haq et al. (2018) elicited E-stim induced network-mediated RGC responses in rd1 mouse retinas at an early stage of degeneration, where the cell bodies of the photoreceptors are still intact, suggesting an early implantation time for affected patients (Haq et al., 2018). Thus, it would be interesting in future to test the E-stim strategies of this thesis at different stages of degeneration.

Sate-of-the-art E-retinal implants considers RGCs as a homogeneous population. This thesis like other studies Ryu et al. (2009); Jensen and RizzoIII (2007, 2008), based their findings on this assumption. However, basic studies have shown a big diversity in RGC types, i.e., functionally RGCs can be classified into 30+ types (Baden et al., 2016). Due to the diversity of retinal output neurons complicates the analysis and characterization of E-stim induced responses. In

recent studies (Ho et al., 2018), it has been shown that different RGC types have different electrical input filters. Also, in Haq et al. (2018), E-stim induced RGC responses were broadly classified into eight different types of RGCs. Overall, the discriminative activation of the retinal basic channels ON,OFF and ON/OFF should be sufficient to promote advanced artificial vision.

As the retinal diseases progress, it is difficult to classify cells based on natural light stimulation conditions. Therefore, basic research classifying RGCs based on E-stim is helpful to understand and implement cell-specific E-stim strategies, the approach in this thesis, already shows that fading effects can be overcome by stimulating all cells in the same fashion, suggesting that the next step for implementing this approach is very close. Meaning, integrating cell-specific E-stim pulses with topologically alternating patterns suggested in this thesis will further help in the improvement of E-stim strategies for E-retinal implants.

Through the experiments in this thesis, fading effects caused by existing conventional E-stim approaches could be reduced by presenting E-stim using 6-e-hexagon in Alternating-step activation. The principle of this thesis was tested in the epiretinal configuration, but this does not confine the possibility of applications only in epiretinal E-implants.

In future, integration of smaller electrodes as opposed to the existing large electrode pitches in epiretinal implants (Humayun et al., 1996; Eckmiller, 1997; Humayun et al., 1999; Yanai et al., 2007; Humayun et al., 2012; Luo and Cruz, 2016) or subretinal E-implants (Chow and Chow, 1997; Zrenner et al., 1999; Rothermel et al., 2009; Zrenner et al., 2010; Mathieson et al., 2012; Stingl et al., 2013, 2015) or suprachoroidal implants (Saunders et al., 2013; Ayton et al., 2014; Bloch et al., 2019) or cortical vision prosthetics (Normann et al., 1999) can be made possible, wherein the image falling onto the photodiode array activates individual pitches in topologically Alternating E-stim manner. In suprachoroidal

implants (Saunders et al., 2013; Ayton et al., 2014; Bloch et al., 2019), where the system is integrated with an external camera which captures the visual scene and transmits it to an external processing unit. Pre-processing of the acquired visual scene is required. Cortical vision prosthetics, surpasses the retina completely and stimulates the higher visual regions in the brain in the hopes of evoking useful visual sensations in blind people (Normann et al., 1999). Since the retina is completely ignored, there has to be an artificial retina which captures the visual scenes and converts them into useful E-stim pulses. These E-stim pulses would have to be presented to the visual cortex through electrodes using Alternating-step activation.

5 Summary

Multielectrode Electrical (E-) stimulation (stim) of the retina is used to restore vision in blind patients suffering from photoreceptor dystrophy. In recent clinical trials, this approach has shown to be beneficial for blind patients to perform daily life tasks. However, the visual perceptions of the patients are limited in spatial and temporal resolution. Repeated E-stim of the retina leads to image fading at E-stim frequencies higher than ~5 Hz. The main focus of this thesis was to investigate a novel E-stim strategy to maintain local visual responses, thereby reducing image fading effects at high E-stim frequency. An electrophysiological set-up with a hexagonal multielectrode array (MEA) was used for experiments on explanted healthy mouse retinas. Preliminary light (L-) stim experiments were conducted to observe the responses induced by a bright Square moving in human microsaccade-like (hMS -like) moves as opposed to the responses induced due to stationary presentation of the Square. The stationary presentation of a Square resulted in a slow reduction of responses, presumably leading to image-fading; if the bright Square moved along the hMS-like sequence, each movement resulted in reoccurring of responses presumably leading to image-refreshing. Initial E-stim experiments were conducted to obtain tuning curves based on the strength of the stimulus. A monomodal cathodic stimulation strength of -1000 mV with a pulse duration of 0.5 ms was used for further experiments. Subsequently, a hexagon electrical pattern with 80 μm diagonal extension was created using 6 MEA-electrodes (6-electrode-hexagon, 6-e-hexagon). The 6-e-hexagon represented an approximate pitch on the Alpha IMS and AMS E-retinal implants (70 μm) used in clinical trials. E-stim induced RGC responses were recorded using other electrodes in the outer circumference of the E-stim electrode. The 6-e-hexagon was activated either in All-at-once, Sequential or in Alternating-step activation modes (analogous to L-stim) at different frequencies (1-20 Hz). Activation of E-stim electrodes in Alternating-step outperformed the Sequential activation by an average of 87.78 % increase in RGC responses, suggesting enhanced image perception. Moreover, at a relatively high E-stim frequency of 10 Hz (100 ms step interval) the Alternating-step activation of E-stim electrodes, allowed to maintain RGC responses (average RGC responses = 8.16±0.27 Hz) for the duration of 90 s. In contrast, the All-at-once activation of E-stim electrodes resulted in fading effects within the first few seconds after E-stim (average RGC responses = 0.70±0.19 Hz). Conceptually, the E-stim presentation with topological electrode-activation instead of All-at-once E-stim activation yields reduced fading-effects even at a relatively high E-stim frequency. This outcome was promising for implementation in E-retinal implants. As an example, an image of a Smiley-face was emulated on the electrode array and detected in the respective responses. In conclusion: Implementation of the Alternating-step activation of electrode arrays overcomes the typical image-fading effects and consequently may increase the temporal and spatial resolution of the artificially induced visual perceptions.

6 Zusammenfassung

Multielektroden-Elektrostimulation (E-stim) der Retina wird verwendet, um Seheindrücke bei blinden Patienten hervorzurufen, die an Photorezeptor-Dystrophie leiden. In jüngsten klinischen Studien wurde gezeigt, dass dieser Ansatz nutzbringend für blinde Patienten bei der Umsetzung täglicher Aufgaben sein kann. Die Seheindrücke der Patienten sind jedoch in ihrer räumlichen und zeitlichen Auflösung begrenzt. Wiederholte E-stim der Retina führt zu einem „Fading" der visuellen Perzeption bei Frequenzen höher als ~5 Hz. Der Hauptfokus dieser Dissertation liegt auf der Untersuchung einer neuen E-stim Strategie zur Aufrechterhaltung lokaler visueller Antworten, welche „Fading"-Effekte bei hoher E-stim Frequenz reduziert. Ein elektrophysiologischer Aufbau mit einem hexagonalen Multielektrodenfeld (engl. Multielectrode Array (MEA)) wurde für Experimente mit explantierten, gesunden Maus-Retinae verwendet. Zunächst wurde ein helles Licht- (L-stim) Quadrat mit Microsakkaden-ähnlichen Bewegungen (ähnlich einer menschlichen Mikrosakkade, hMS-ähnlich) mit der Präsentation eines stationären Quadrats verglichen. Die stationäre Präsentation resultierte in einer langsam fortschreitenden Minderung von RGC-Antworten, was vermutlich zum Verlust des Seheindrucks („Fading") führt. Bewegte sich ein L-stim Quadrat entlang der hMS-ähnlichen Sequenz, so resultierte jede Bewegung in einem Wiederauftreten von RGC-Antworten, was vermutlich zu einer Auffrischung der visuellen Perzeption führt. Um dies nun mit E-stim-Effekten zu vergleichen wurden statt Licht monomodale, kathodische Stimuli von -1000 mV mit einer Pulsweite von 0.5 ms verwendet. Anschließend wurde ein Hexagon mit einer Diagonalen von 80 μm durch 6 MEA Elektroden abgebildet. Das Hexagon repräsentierte eine ungefähre Elektroden-Dichte der Alpha IMS und AMS E-Retina-Implantate (70 μm) die in klinischen Studien eingesetzt wurden. E-stim induzierte RGC-Antworten wurden durch andere Elektroden in der Umgebung der E-stim Elektrode aufgezeichnet. Die Elektroden des Hexagons wurden entweder durch den „All-at-once-", „Sequential-" oder den „Alternating-step-Modus" (analog zu L-stim) bei verschiedenen Frequenzen (1-20 Hz) aktiviert. Die Aktivierung der E-stim Elektroden im Alternating-step-Modus führte im Vergleich zur Sequential Aktivierung zu einem Anstieg der RGC-Antworten von durchschnittlich 87.78 %, was auf eine gesteigerte visuelle Wahrnehmung schließen lässt. Bei relativ hohen E-stim Frequenzen von 10 Hz erlaubte die Aktivierung über Alternating-step die Aufrechterhaltung von RGC-Antworten für die Dauer von 90 s. Die All-at-once Aktivierung der E-stim Elektroden hingegen resultierte in „Fading"-Effekten innerhalb der ersten, wenigen Sekunden nach Beginn der E-stim. Die E-stim Präsentation mit topologisch-sequentieller Elektroden-Aktivierung anstelle von zeitgleicher E-stim Aktivierung liefert also deutlich reduzierte visuelle „Fading"-Effekte, selbst bei einer relativ hohen E-stim Frequenz. Dieses Ergebnis ist vielversprechend für eine Implementierung in E-Retina-Implantaten. Auf dem Elektrodenfeld wurde beispielhaft auch ein Bild eines Smiley-Gesichts emuliert und in den entsprechenden Antworten detektiert. Durch eine Implementierung der Alternating-step Aktivierung in Elektrodenfeldern können demnach die typischen „Fading"-Effekte überwunden werden. Somit könnte diese Art der Aktivierung die zeitliche und räumliche Auflösung der durch elektronische Implantate vermittelten visuellen Perzeptionen erhöhen.

6 Abbreviations

PhR	Photoreceptor
RGC	Retinal Ganglion Cell
AC	Amacrine Cell
BC	Bipolar Cell
$E-stim$	Electrical stimulation
$L-stim$	Light stimulation
MCS	Multi Channel Systems MCS GmbH, Reutlingen, Germany
MEA	Multielectrode array
$ACSF$	Artificial Cerebrospinal Fluid
TMW	The MathWorks, Inc., Natick, MA, USA
$hMS-like$	human Microsaccade - like
V	Voltage
A	Amperes
C	Coulombs
$6-e-hexagon$	6 - electrode - hexagon

7 Bibliography

Abd, A. J., R. K. Kanwar, and J. R. Kanwar

2017. Aged macular degeneration: current therapeutics for management and promising new drug candidates. *Drug Discovery Today*, 22:1671–1679.

Ahissar, E., A. Arieli, M. Fried, and Y. Bonneh

2016. On the possible roles of microsaccades and drifts in visual perception. *Vision Research*, 118:25–30.

Ahn, K. N., J. Y. Ahn, J. hyung Kim, K. Cho, K. in Koo, S. S. Senok, and Y. S. Goo

2015. Effect of stimulus waveform of biphasic current pulse on retinal ganglion cell responses in retinal degeneration (rd1) mice. *The Korean journal of physiology & pharmacology : official journal of the Korean Physiological Society and the Korean Society of Pharmacology*, 19:167–175.

Ayton, L. N., P. J. Blamey, R. H. Guymer, C. D. Luu, D. A. X. Nayagam, N. C. Sinclair, M. N. Shivdasani, J. Yeoh, M. F. McCombe, R. J. Briggs, N. L. Opie, J. Villalobos, P. N. Dimitrov, M. Varsamidis, M. A. Petoe, C. D. McCarthy, J. G. Walker, N. Barnes, A. N. Burkitt, C. E. Williams, R. K. Shepherd, and P. J. Allen

2014. First-in-human trial of a novel suprachoroidal retinal prosthesis. *PLoS One*, 9:e115239.

Baden, T., P. Berens, K. Franke, M. R. Roson, M. Bethge, and T. Euler

2016. The functional diversity of retinal ganglion cells in the mouse. *Nature*, 529:345–350.

Bahill, A. T., M. R. Clark, and L. Stark

1975. The main sequence, a tool for studying human eye movements. *Mathematical Biosciences*, 24:191–204.

Barlow, H. B., R. Hill, and W. Levick

1964. Retinal ganglion cells responding selectively to direction and speed of image motion in the rabbit. *Journal of physiology*, 173:377–407.

Behrend, M. R., A. K. Ahuja, M. S. Humayun, R. H. Chow, and J. D. Weiland

2011. Resolution of the epiretinal prosthesis is not limited by electrode size. *IEEE Transactions on Neural Systems and Rehabilitation Engineering*, 19:436 – 442.

Bloch, E., Y. Luo, and L. da Cruz

2019. Advances in retinal prosthesis systems. *Therapeutic Advances in Ophthalmology*, 11:1–16.

Boinagrov, D., S. Pangratz-Fuehrer, G. Goetz, and D. Palanker

2014. Selectivity of direct and network-mediated stimulation of the retinal ganglion cells with epi-, sub- and intra-retinal electrodes. *Journal of Neural Engineering*, 11.

Brainard, D. H.

1997. The psychophysics toolbox. *Spatial Vision*, 10:433–436.

Brindley, G. S. and W. S. Lewin

1968. The sensations produced by electrical stimulation of the visual cortex. *The journal of physiology*, 196:479–493.

Busskamp, V., S. Picaud, J. A. Sahel, and B. Roska

2012. Optogenetic therapy for retinitis pigmentosa. *Gene Therapy*, 19:169–175.

Butterwick, A., A. Vankov, P. Huie, K. Vijayraghavan, J. Loudin, and D. Palanker

2007. Progress towards a high-resolution retinal prosthesis. *Ophthalmic Technologies*, 6426A.

Carcieri, S. M., A. L. Jacobs, and S. Nirenberg

2003. Classification of retinal ganglion cells: a statistical approach. *Journal of Neurophysiology*, 90:1704–1713.

Celik, M. E. and I. Karagoz

2018. Comparison of monophasic and biphasic electrical stimulation by using temporal analysis for different inter-electrocde spacings in hexagonal arrays. *Arabian Journal of Science and Engineering*, 43.

Cepko, C.

2014. Intrinsically different retinal progenitor cells produce specific types of progeny. *Nat Rev Neurosci*, 15:615–27.

Chang, B.

2013. Mouse models for studies of retinal degeneration and diseases. *Methods in molecular biology (Clifton, N.J.)*, 935:27–39.

Chen, S.-J., M. Mahadevappa, R. Roizenblatt, J. Weiland, and M. Humayun

2006. Neural responses elicited by electrical stimulation of the retina. *Transactions of the American Ophthalmological Society*, 104:252–9.

Chow, A. Y. and V. Y. Chow

1997. Subretinal electrical stimulation of the rabbit retina. *Neuroscience Letters*, 225:13–16.

Coleman, H. R., C.-C. Chan, F. L. FerrisIII, and E. Y. Chew

2008. Age-related macular degeneration. *Lancet*, 372:1835–45.

Coombs, J. L., D. A. V. D. List, G. Wang, and L. M. Chalupa

2006. Morphological properties of mouse retinal ganglion cells. *Neuroscience*, 140:123–136.

Coombs, J. L., D. V. D. List, and L. M. Chalupa

2007. Morphological properties of mouse retinal ganglion cells during postnatal development. *Journal of Comparative Neurology*, 503:803–814.

Daschner, R., A. Rothermel, R. Rudorf, S. Rudorf, and A. Stett

2018. Functionality and performance of the subretinal implant chip alpha ams. *Sensors and Materials*, 30:179–192.

Devries, S. H. and D. A. Baylor

1997. Mosaic arrangement of ganglion cell receptive fields in rabbit retina. *Journal of Neurophysiology*, 78:2048–2060.

Ditchburn, R. W. and B. L. Ginsborg

1952. Vision with a stabilized retinal image. *Nature*, 170:36–37.

Dowling, J. E.

1987. Retina: An approachable part of the brain. *Harvard University Press, Cambridge, MA*.

Drasdo, N. and C. W. Fowler

1974. Non-linear projection of the retinal image in a wide-angle schematic eye. *The British journal of ophthalmology*, 58:709–14.

Eckmiller, R.

1997. Learning retina implants with epiretinal contacts. *Ophthalmic Research*, 29:281–289.

Endo, T., T. Fujikado, M. Hirota, H. Kanda, T. Morimoto, and K. Nishida

2018. Light localization with low-contrast targets in a patient implanted with a suprachoroidal-transretinal stimulation retinal prosthesis. *Graefes Archive for Clinical and Experimental Ophthalmology*, 256:1723–1729.

Euler, T., P. B. Detwiler, and W. Denk

2002. Directionally selective calcium signals in dendrites of starburst amacrine cells. *Nature*, 418:845–852.

Euler, T., S. Haverkamp, T. Schubert, and T. Baden

2014. Retinal bipolar cells: elementary building blocks of vision. *Nature Reviews Neuroscience*, 15:507–519.

Farrow, K. and R. H. Masland

2011. Physiological clustering of visual channels in the mouse retina. *Journal of Neurophysiology*, 105:1516–1530.

Field, G. D. and E. J. Chichilnisky

2007. Information processing in the primate retina: Circuitry and coding. *Anual Review of Neuroscience*, 30:1–30.

Fornos, A. P., J. Sommerhalder, L. da Cruz, J. A. Sahel, S. Mohand-Said, F. Hafezi, and M. Pelizzone

2012. Temporal properties of visual perception on electrical stimulation of the retina. *Investigative Ophthalmology & Visual Science*, 53:2720–2731.

Freeman, D. K. and S. I. Fried

2011. Multiple components of ganglion cell desensitization in response to prosthetic stimulation. *Journal of Neural Engineering*, 8.

Freeman, D. K., J. F. R. III, and S. I. Fried

2011. Encoding visual information in retinal ganglion cells with prosthetic stimulation. *Journal of Neural Engineering*, 8.

Fu, Y. and K.-W. Yau

2007. Phototransduction in mouse rods and cones. *Pflügers Archiv - European Journal of Physiology*, 454:805–19.

Fuchs, A. F.

1967. Saccadic and smooth pursuit eye movements in the monkey. *The Journal of Physiology*, 191:609–631.

Ghosh, K. K., S. Bujan, S. Haverkamp, A. Feigenspan, and H. Wässle

2004. Types of bipolar cells in the mouse retina. *Journal of comparative neurology*, 469:70–82.

Gollisch, T. and M. Meister

2010. Eye smarter than scientists believed: Neural computations in circuits of the retina. *Neuron*, 65:150–164.

Greschner, M., M. Bongard, P. Rujan, and J. Ammermüller

2002. Retinal ganglion cell synchronization by fixational eye movements improves feature estimation. *Nature neuroscience*, 5:341–347.

Hack, I., L. Peichl, and J. H. Brandstätter

1999. An alternative pathway for rod signals in the rodent retina: Rod photoreceptors, cone bipolar cells, and the localization of glutamate receptors. *Proceedings of the National Academy of Sciences of the United States of America*, 96:14130–5.

Hafed, Z. M., K. Stingl, K.-U. Bartz-Schmidt, F. Gekeler, and E. Zrenner

2016. Oculomotor behavior of blind patients seeing with a subretinal visual implant. *Vision Research*, 118:119–131.

Haq, W., J. Dietter, and E. Zrenner

2018. Electrical activation of degenerated photoreceptors in blind mouse retina elicited network-mediated responses in different types of ganglion cells. *Scientific Reports*, 8.

Hartong, D. T., E. L. Berson, and T. P. Dryja

2006. Retinitis pigmentosa. *Ophthalmic Research*, 368:1795–1809.

Hicks, D. and J. Sahel

1999. The implications of rod-dependent cone survival for basic and clinical research. *Investigative Ophthalmology & Visual Science December*, 40:3071–3074.

Ho, E., H. Lorach, G. Goetz, F. Laszlo, X. Lei, T. Kamins, J.-C. Mariani, A. Sher, and D. Palanker

2018. Temporal structure in spiking patterns of ganglion cells defines perceptual thresholds in rodents with subretinal prosthesis. *Scientific Reports*, 8.

Humayun, M. S., E. de Juan Jr, G. Dagnelie, R. J. Greenberg, R. H. Propst, and D. H. Phillips

1996. Visual perception elicited by electrical stimulation of retina in blind humans. *Arch Ophthalmology*, 114:40–46.

Humayun, M. S., J. D. Dorn, L. Cruz, G. Dagnelie, J.-A. Sahel, P. E. Stanga, A. V. Cideciyan, J. L. Duncan, D. Eliott, E. Filley, A. C. Ho, A. Santos, A. B. Safran, A. Arditi, L. V. D. Priore, R. J. Greenberg, and A. I. S. Group

2012. Interim results from the international trial of second sight's visual prosthesis. *Ophthalmology*, 119:779–788.

Humayun, M. S., E. J. Jr, J. D. Weiland, G. Dagnelie, S. Katona, R. Greenberg, and S. Suzuki

1999. Pattern electrical stimulation of the human retina. *Vision Research*, 39:2569–2576.

Jacobson, S. G. and A. V. Cideciyan

2010. Treatment possibilities for retinitis pigmentosa. *The NEW ENGLAND JOURNAL of MEDICINE*, 363:1669–1671.

Jensen, R. J. and J. F. RizzoIII

2007. Responses of ganglion cells to repetitive electrical stimulation of the retina. *Journal of Neural Engineering*, 4.

Jensen, R. J. and J. F. RizzoIII

2008. Activation of retinal ganglion cells in wild-type and rd1 mice through electrical stimulation of the retinal neural network. *Vision Research*, 48:1562–1568.

Jones, B. W., R. L. Pfeiffer, W. D. Ferrell, C. B. Watt, M. Marmor, and R. E. Marc

2016. Retinal remodeling in human retinitis pigmentosa. *Experimental Eye Research*, 150:149–165.

Kocur, I. and S. Resnikoff

2002. Visual impairment and blindness in europe and their prevention. *The British journal of ophthalmology*, 86:716–722.

Kong, J.-H., D. R. Fish, R. L. Rockhill, and R. H. Masland

2005. Diversity of ganglion cells in the mouse retina unsupervised morphological classification and its limits. *Jouranal of Comparative Neurology*, 489:293–310.

Krishnamoorthy, V., M. Weick, and T. Gollisch

2017. Sensitivity to image recurrence across eye-movement-like image transitions through local serial inhibition in the retina. *eLife*, 6:1–25.

Land, M. F.

1999. Motion and vision: Why animals move their eyes. *Journal of Comparative Physiology*, 185:341–352.

LanYue, J. D. Weiland, B. Roska, and M. S. Humayuna

2016. Retinal stimulation strategies to restore vision: Fundamentals and systems. *Progress in Retinal and Eye Research*, 53:21–47.

Lettvin, J. Y., H. R. Maturana, W. S. McCulloch, and W. H. Pitts

1959. What the frog's eye tells the frog's brain. *Proceedings of the IRE*, 47:1940–1951.

Luo, Y. H.-L. and L. Cruz

2016. The argus ii retinal prosthesis system. *Progress in Retinal and Eye Research*, 50:89–107.

Martinez-Conde, S. and S. L. Macknik

2008. Fixational eye movements across vertebrates: Comparative dynamics, physiology, and perception. *Journal of Vision*, 8:1–16.

Martinez-Conde, S., S. L. Macknik, and D. H. Hubel

2004. The role of fixational eye movements in visual perception. *Nat Rev Neurosci*, 5:229–40.

Martinez-Conde, S., S. L. Macknik, X. G. Troncoso, and T. A. Dyar

2006. Microsaccades counteract visual fading during fixation. *Neuron*, 2:297–305.

Martinez-Conde, S., S. L. Macknik, X. G. Troncoso, and D. H. Hubel

2009. Microsaccades: a neurophysiological analysis. *Trends in Neurosciences*, 32:463–475.

Masland, R. H.

2001. Neuronal diversity in the retina. *Current Opinion in Neurobiology*, 11:431–436.

Masland, R. H.

2012a. The neuronal organization of the retina. *Neuron*, 76:266–280.

Masland, R. H.

2012b. The tasks of amacrine cells. *Visual neuroscience*, 29:3–9.

Mathieson, K., J. Loudin, G. Goetz, P. Huie, L. Wang, T. I. Kamins, L. Galambos, R. Smith, J. S. Harris, A. Sher, and D. Palanker

2012. Photovoltaic retinal prosthesis with high pixel density. *Nature Photonics*, 6:391–397.

Matteucci, P. B., A. Barriga-Rivera, C. D. Eiber, N. H. Lovell, J. W. Morley, and G. J. Suaning

2016. The effect of electric cross-talk in retinal neurostimulation. *Investigative Ophthalmology & Visual Science*, 57:1031–1037.

Mokwa, W., M. Goertz, C. Koch, I. Krisch, H. K. Trieu, and P. Walter

2008. Intraocular epiretinal prosthesis to restore vision in blind humans. *IEEE*.

Nakano, Y., Y. Terasawa, H. Kanda, J. Ohta, H. Sawai, and T. Fujikado

2018. Effects of asymmetric electrical pulse on retinal excitement for retinal prostheses. *Sensors and Materials*, 30:315–326.

Nirenberg, S. and M. Meister

1997. The light response of retinal ganglion cells is truncated by a displaced amacrine circuit. *Neuron*, 18:637–650.

Normann, R. A., E. M. Maynard, P. J. Rousche, and D. J. Warren

1999. A neural interface for a cortical vision prosthesis. *Vision Research*, 39:2577–2587.

Onnela, N., H. Takeshita, Y. Kaiho, T. Kojima, R. Kobayashi, T. Tanaka, and J. Hyttinen

2011. Comparison of electrode materials for use of retinal prosthesis. *Bio-medical materials and engineering*, 21:83–97.

Pelli, D. G.

1997. The videotoolbox software for visual psychophysics: Transforming numbers into movies. *Spatial Vision*, 10:437–442.

Pritchard, R. M.

1961. Stabilized images on the retina. *Scientific American, INC*, 204:72–78.

Prusky, G. T., P. W. R. West, and R. M. Douglas

2000. Behavioral assessment of visual acuity in mice and rats. *Vision Research*, 40:2201–2209.

Purves, D., G. J. Augustine, D. Fitzpatrick, L. C. Katz, A.-S. LaMantia, J. O. McNamara, and S. M. Williams

2001. Neuroscience. 2nd edition. functional specialization of the rod and cone systems. *Sunderland (MA): Sinauer Associates*.

Remtulla, S. and P. E. Hallett

1985. A schematic eye for the mouse, and comparisons with the rat. *Science Direct*, 25:21–31.

Rockhill, R. L., F. J. Daly, M. A. MacNeil, S. P. Brown, and R. H. Masland

2002. The diversity of ganglion cells in a mammalian retina. *Journal of Neuroscience*, 22:3831–3843.

Rodieck, R. W.

1998. The first steps in seeing. *Sinauer Associates, Inc., Publishers Sunderland, Massachusetts*, 51:245–271.

Rothermel, A., L. Liu, N. P. Aryan, M. Fischer, J. Wuenschmann, S. Kibbel, and A. Harscher

2009. A cmos chip with active pixel array and specific test features for subretinal implantation. *IEEE Journal of Solid-State Circuits*, 44:290–300.

Ryu, S. B., J. H. Ye, J. S. Lee, Y. S. Goo, C. H. Kim, and K. H. Kim

2009. Electrically-evoked neural activities of rd1 mice retinal ganglion cells by repetitive pulse stimulation. *The Korean journal of physiology & pharmacology : official journal of the Korean Physiological Society and the Korean Society of Pharmacology*, 13:443–8.

Sahni, J. N., M. Angi, C. Irigoyen, F. Semeraro, M. R. Romano, and F. Parmeg-

giani

2011. Therapeutic challenges to retinitis pigmentosa: From neuroprotection to gene therapy. *Current genomics*, 12:276–84.

Sakatani, T. and T. Isa

2007. Quantitative analysis of spontaneous saccade-like rapid eye movements in c57bl/6 mice. *Neuroscience Research*, 58:324–331.

Sancho-Pelluz, J., B. Arango-Gonzalez, S. Kustermann, F. J. Romero, T. van Veen, E. Zrenner, P. Ekström, and F. Paquet-Durand

2008. Photoreceptor cell death mechanisms in inherited retinal degeneration. *Molecular Neurobiology*, 38:253–269.

Saunders, A. L., C. E. Williams, W. Heriot, R. Briggs, J. Yeoh, D. A. Nayagam, M. McCombe, J. Villalobos, O. Burns, C. D. Luu, L. N. Ayton, M. McPhedran, N. L. Opie, C. McGowan, R. K. Shepherd, R. Guymer, and P. J. Allen

2013. Development of a surgical procedure for implantation of a prototype suprachoroidal retinal prosthesis. *Clinical and Experimental Ophthalmology*, 42:665–674.

Schaeffel, F.

2017. Sehleistungen von tieren und menschen im vergleich. *Der Ophthalmologe*, 114:976–977.

Schatz, A., T. Röck, L. Naycheva, G. Willmann, B. Wilhelm, T. Peters, K. U. Bartz-Schmidt, E. Zrenner, A. Messias, and F. Gekeler

2011. Transcorneal electrical stimulation for patients with retinitis pigmentosa: A prospective, randomized, sham-controlled exploratory study. *Investigative ophthamology & visual science*, 52:4485–4496.

Shekhar, K., S. W. Lapan, I. E. Whitney, N. M. Tran, E. Z. Macosko, M. Kowalczyk, X. Adiconis, J. Z. Levin, J. Nemesh, M. Goldman, S. A. McCarroll, C. L. Cepko, A. Regev, and J. R. Sanes

2016. Comprehensive classification of retinal bipolar neurons by single-cell transcriptomics. *Cell*, 166:1308–1323.

Shyu, J.-S., M. Maia, J. D. Weiland, T. OHearn, S.-J. Chen, E. Margalit, and M. S. Humayun

2006. Electrical stimulation in isolated rabbit retina. *IEEE Transactions on Neural Systems and Rehabilitation Engineering*, 14:290–298.

Sim, S. L., R. J. Szalewski, L. J. Johnson, L. E. Akah, L. E. Shoemaker, W. B. Thoreson, and E. Margalitc

2014. Simultaneous recording of mouse retinal ganglion cells during epiretinal or subretinal stimulation. *Vision Research*, 101:41–50.

Singh, M. S., P. C. Issa, R. Butler, C. Martin, D. M. Lipinski, S. Sekaran, A. R. Barnard, and R. E. MacLarena

2013. Reversal of end-stage retinal degeneration and restoration of visual function by photoreceptor transplantation. *Proceedings of the National Academy of Sciences of the United States of America*, 110:1101–6.

Soucy, E., Y. Wang, S. Nirenberg, J. Nathans, and M. Meister

1998. A novel signaling pathway from rod photoreceptors to ganglion cells in mammalian retina. *Neuron*, 21:481–493.

Stasheff, S. F.

2007. Emergence of sustained spontaneous hyperactivity and temporary preservation of off responses in ganglion cells of the retinal degeneration (rd1) mouse. *Journal of neurophysiology*, 99:1408–1421.

Sterling, P. and J. B. Demb

2004. Retina. in the synaptic organization of the brain, g.m. shepherd, ed. *New York: Oxford University Press*, Pp. 217–269.

Stett, A., W. Barth, S. Weiss, H. Haemmerle, and E. Zrenner

2000. Electrical multisite stimulation of the isolated chicken retina. *Vision research*, 40:1785–1795.

Stett, A., A. Mai, and T. Herrmann

2007. Retinal charge sensitivity and spatial discrimination obtainable by subretinal implants: key lessons learned from isolated chicken retina. *Journal of Neural Engineering*, 4:S7–S16.

Stingl, K., K. U. Bartz-Schmidt, D. Besch, A. Braun, A. Bruckmann, F. Gekeler, U. Greppmaier, S. Hipp, G. Hörtdörfer, C. Kernstock, A. Koitschev, A. Kusnyerik, H. Sachs, A. Schatz, K. T. Stingl, T. Peters, B. Wilhelm, and E. Zrenner
2013. Artificial vision with wirelessly powered subretinal electronic implant alpha-ims. *Proceedings of the royal society B*, 280.

Stingl, K., K. U. Bartz-Schmidt, D. Besch, C. K. Chee, C. L. Cottriall, F. Gekeler, M. Groppe, T. L. Jackson, R. E. MacLaren, A. Koitschev, A. Kusnyerik, J. Neffendorf, J. Nemeth, M. A. N. Naeem, T. Peters, J. D. Ramsden, H. Sachs, A. Simpson, M. S. Singh, B. Wilhelm, D. Wong, and E. Zrenner
2015. Subretinal visual implant alpha ims - clinical trial interim report. *Vision Research*, 111:149–160.

Stingl, K., R. Schippert, K. Bartz-Schmidt, D. Besch, C. Cottriall, T. Edwards, F. Gekeler, U. Greppmaier, K. Kiel, A. Koitschev, L. Kuehlewein, R. MacLaren, J. Ramsden, J. Roider, A. Rothermel, H. Sachs, G. Schroeder, J. Tode, N. Troelenberg, and E. Zrenner
2017. Interim results of a multicenter trial with the new electronic subretinal implant alpha ams in 15 patients blind from inherited retinal degenerations. *Frontiers in Neuroscience*, 11.

Sümbül, U., S. Song, K. McCulloch, M. Becker, B. Lin, J. R. Sanes, R. H. Masland, and H. S. Seung
2014. A genetic and computational approach to structurally classify neuronal types. *Nature communications*, 5.

Sun, W., N. Li, and S. He
2002. Large-scale morphological survey of mouse retinal ganglion cells. *Journal of Comparative Neurology*, 451:115–126.

Tsukamoto, Y. and N. Omi
2017. Classification of mouse retinal bipolar cells: Type-specific connectivity with special reference to rod-driven aii amacrine pathways. *Frontiers in neuroanatomy*, 11.

Twyford, P. and S. Fried

2015. The retinal response to sinusoidal electrical stimulation. *IEEE Transactions on Neural Systems and Rehabilitation Engineering*, 24.

van Alphen, B., B. H. J. Winkelman, and M. A. Frens

2010. Three-dimensional optokinetic eye movements in the c57bl/6j mouse. *Visual Psychophysics and Physiological Optics*, 51:623–630.

Völgyi, B., S. Chheda, and S. A. Bloomfield

2009. Tracer coupling patterns of the ganglion cell subtypes in the mouse retina. *Journal of Comparative Neurology*, 5:664–87.

Wang, G.-Y., L. C. Liets, and L. M. Chalupa

2001. Unique functional properties of on and off pathways in the developing mammalian retina. *The Journal of Neuroscience*, 21:4310–4317.

Wässle, H.

2004. Parallel processing in the mammalian retina. *Nature Reviews Neuroscience*, 5:747–757.

Webvision

. Webvision. `https://webvision.med.utah.edu`. Accessed: 2019-11-09.

Werblin, F. S. and J. E. Dowling

1969. Organization of the retina of the mudpuppy. *Journal of Neurophysiology*, 32:339–355.

Wilke, R. G. H., G. K. Moghadam, N. H. Lovell, G. J. Suaning, and S. Dokos

2011. Electric crosstalk impairs spatial resolution of multi-electrode arrays in retinal implants. *Journal of Neural Engineering*, 8.

Yanai, D., J. D. Weiland, M. Mahadevappa, R. J. Greenberg, I. Fine, and M. S. Humayun

2007. Visual performance using a retinal prosthesis in three subjects with retinitis pigmentosa. *American Journal of Ophthalmology*, 143:820–827.

Yarbus, A. L.

1967. Eye movements and vision. *Plenum Press, New York*.

Zhang, Y., I.-J. Kim, J. R. Sanes, and M. Meister

2012. The most numerous ganglion cell type of the mouse retina is a selective feature detector. *Proc. Natl. Acad. Sci.*, 109:E2391–E2398.

Zrenner, E.

2002. Will retinal implants restore vision? *Science*, 295:1022–1025.

Zrenner, E.

2013. Fighting blindness with microelectronics. *Science Translational Medicine*, 5:310–315.

Zrenner, E., K. U. Bartz-Schmidt, H. Benav, D. Besch, A. Bruckmann, V.-P. Gabel, F. Gekeler, U. Greppmaier, A. Harscher, S. Kibbel, J. Koch, A. Kusnyerik, T. Peters, K. Stingl, H. Sachs, A. Stett, P. Szurman, B. Wilhelm, and R. Wilke

2010. Subretinal electronic chips allow blind patients to read letters and combine them to words. *Proceedings of the royal society B*, 278:1489–1497.

Zrenner, E., A. Stett, S. Weiss, R. B. Aramant, E. Guenther, K. Kohler, K. D. Miliczek, M. Seiler, and H. Haemmerle

1999. Can subretinal microphotodiodes successfully replace degenerated photoreceptors? *Vision Research*, 39:2555–2567.

8 List of figures

9 Acknowledgements

I would like to thank my supervisors Prof. Dr. med. Dr. h.c. mult. Eberhart Zrenner and Prof. Dr. Hanspeter Mallot for being supportive and supervising my Thesis work. I would also like to thank Dr. Wadood Haq for being the immediate supervisor, helping and supporting me throughout this scientific journey. Additionally, I thank Achim Speck for the collaboration and support all through the years of doctoral studies. Also, I would like to thank Kriemhilde and Peter Speck. Greatest thanks I would like to express to my parents Dr. Jayashree Rao and Basavaraju C, my Brother Ullas Basavaraju without whose undying support this would not have been possible. Last but not the least I would like to thank all my extended family and friends for always being around when needed. Finally, I would like to thank the Tistou & Charlotte Kerstan Stiftung for funding this project.